NASA CONTRACTOR REPORT

NASA CR-1471

EVALUATION OF A LOW SIDELOBE PHASED ARRAY ANTENNA

by Charles E. Profera, Jr.

Prepared by
RCA DEFENSE ELECTRONIC PRODUCTS
Moorestown, N. J.
for Electronics Research Center

NATIONAL AERONAUTICS AND SPACE ADMINISTRATION • WASHINGTON, D. C. • NOVEMBER 1969

EVALUATION OF A LOW SIDELOBE PHASED ARRAY ANTENNA

By Charles E. Profera, Jr.

Prepared under Contract No. NAS 12-149 by
RCA DEFENSE ELECTRONIC PRODUCTS
Moorestown, N.J.

for Electronics Research Center

NATIONAL AERONAUTICS AND SPACE ADMINISTRATION

For sale by the Clearinghouse for Federal Scientific and Technical Information
Springfield, Virginia 22151 – Price $3.00

CONTENTS

ILLUSTRATIONS

ILLUSTRATIONS (Continued)

ILLUSTRATIONS (Continued)

EVALUATION OF A LOW SIDELOBE PHASED ARRAY ANTENNA

BY

CHARLES E. PROFERA, JR.

RCA
DEFENSE ELECTRONIC PRODUCTS

SUMMARY

The radiation characteristics of a phased array antenna consisting of low-sidelobe line source elements combined through a dual mode linear power combiner have been determined as a function of both frequency and scan angle. Antenna pattern contour data obtained from a Ku-band experimental array model indicates very low sidelobe power content resulting in extremely high beam efficiency. Single plane scanning to $\pm 60^{o}$ has been accomplished with no visible grating lobe formation or array resonance effects.

INTRODUCTION

This report discusses the performance of a low sidelobe phased array which is designed to provide an approximate three-degree pencil beam with a single plane scan capability of $\pm 60^{o}$. The array consists of H-plane sectoral horn line source elements and a dual mode E-plane sectoral horn power combiner, the analysis and performance of which have been the subject of previous reports (Ref. 1, 2, 3).

The subjects to be discussed in this report concern both testing and evaluation of the performance of a complete 50-element prototype array model operable at Ku-band.

ARRAY CONFIGURATION

The array antenna to be discussed in this report is primarily intended to be an instrument for radiometric measurement. In this sense, it is used exclusively as a receiving antenna. However, in order to adequately discuss the array configuration and the techniques by which the array derives its low sidelobe characteristics, it is advantageous to describe the array as a transmitting antenna.

The Ku-band 50-element low sidelobe array consists of three major sections. In the direction of transmitted signal flow, these are: the E-plane dual-mode lens compensated power combiner horn with mode exciter; the phasing section, consisting of 50 stacked waveguides which accommodate dielectric phase shifters; and the array of 50 lens compensated H-plane sectoral horn line source elements. The complete assembly is shown in Figure 1. The low sidelobe array is designed to operate over a 10 per cent frequency band centered at 16.0 GHz.

Power Combiner Horn

The power combiner is a lens-compensated E-plane sectoral horn which provides for distribution of an input signal to the 50 array elements. Dual mode operation of the horn is utilized to provide a tapered output field distribution suitable for low sidelobe array plane pattern characteristics. The H_{10} and H_{12} sectoral horn modes are generated in the horn and phased by the horn to produce the tapered E-plane distribution required at its output (Ref. 1). A cylindrical dielectric lens is employed at the combiner horn output to produce a planar phase distribution of the field. The power combiner horn with the cylindrical lens is shown in Figure 2.

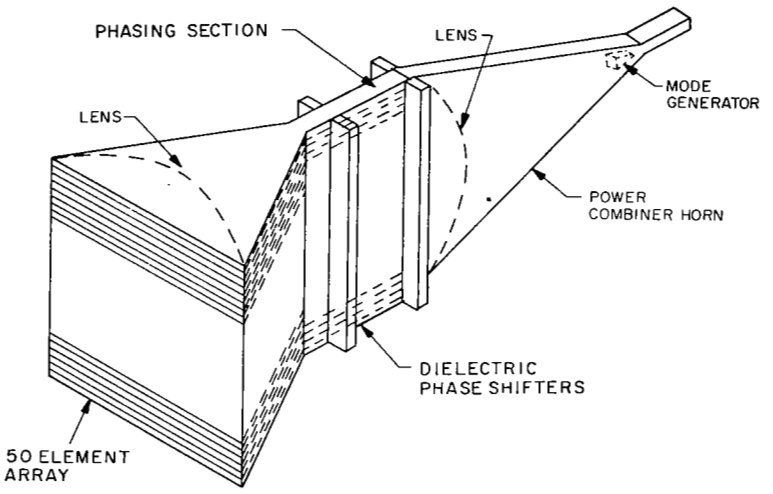

Figure 1(a). Low-Sidelobe Array Configuration

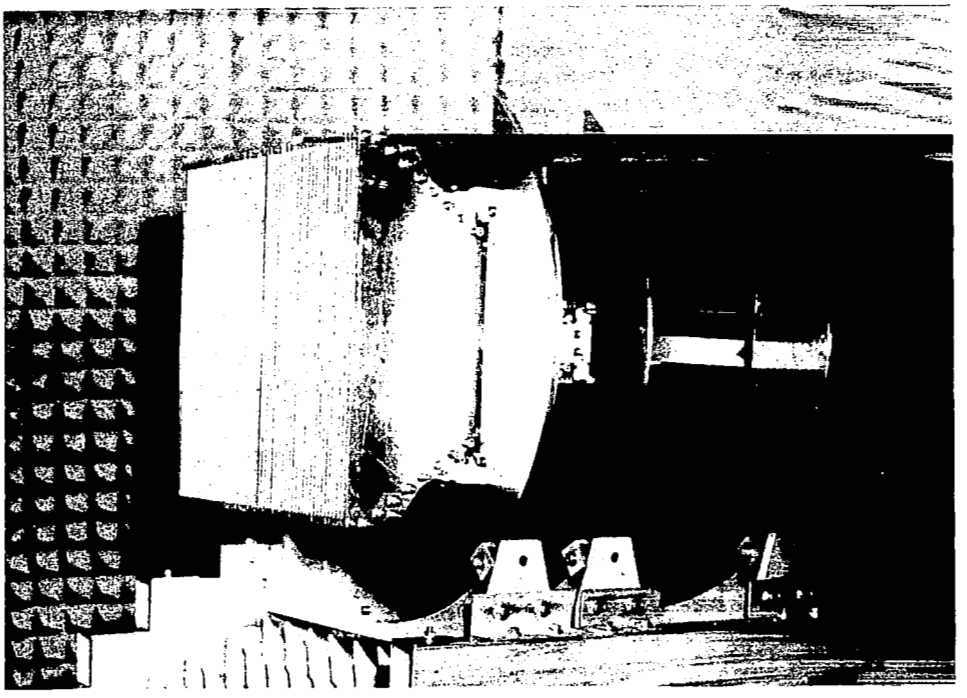

Figure 1(b). Low Sidelobe Array

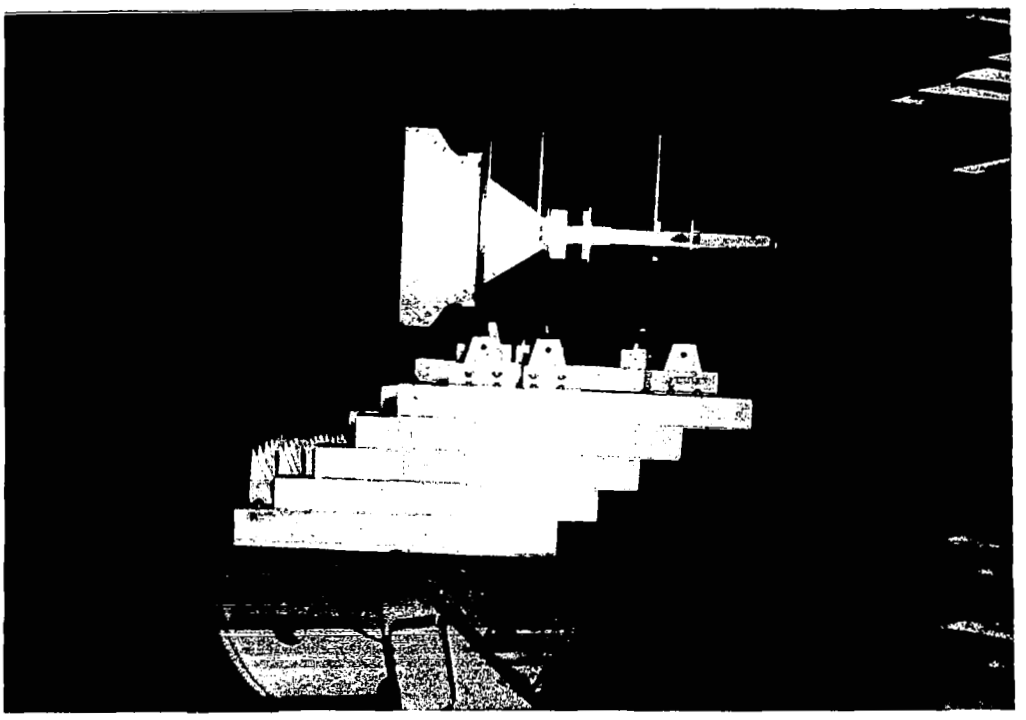

Figure 1(c). Low Sidelobe Array Side View

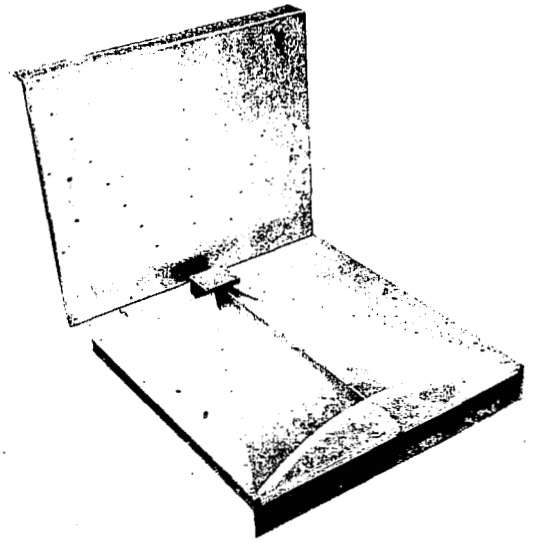

Figure 2. Power Combiner Horn With Dielectric Lens

Impedance matching transformers are made an integral part of both input and output lens surfaces. The technique used for lens surface impedance matching requires a ridge in the plane of incidence, and is described by Morita and Cohn (Ref. 4). The transformer on the input surface of the lens provides an impedance match between the sectoral horn and the dielectric lens region. The matching transformer on the output lens surface provides an impedance match between the lens-compensated combiner horn output and the 50-element input of the phasing section.

Phasing Section and Phase Shifters

The phasing section is a linear arrangement of 50 waveguides which is designed to physically match the array input, accommodate the dielectric phase shifters and divide the output of the power combiner horn 50 ways. The phasing section is shown in Figure 3. This section is provided independently of the array and combiner solely to permit simple changes to be made to the phase shifter configuration for selective beam steering.

Beam steering is accomplished using dielectric phase shifters in each of the 50 phasing section ports. Five-bit dielectric phase shifters were employed to simulate five-bit latching ferrite phase shifters. A five-bit design is required to restrict sidelobes due to phase quantization error to less than −30 dB (Ref. 5). The phase increment for this choice is $\pi/16$ radians or 11−1/4 degrees. The dielectric phase shifters are fabricated from Emerson-Cuming Stycast 0005 with $\epsilon_r = 2.55$. A complete 5-bit phase shifter assembly with matching impedance transformers is shown in Figure 4.

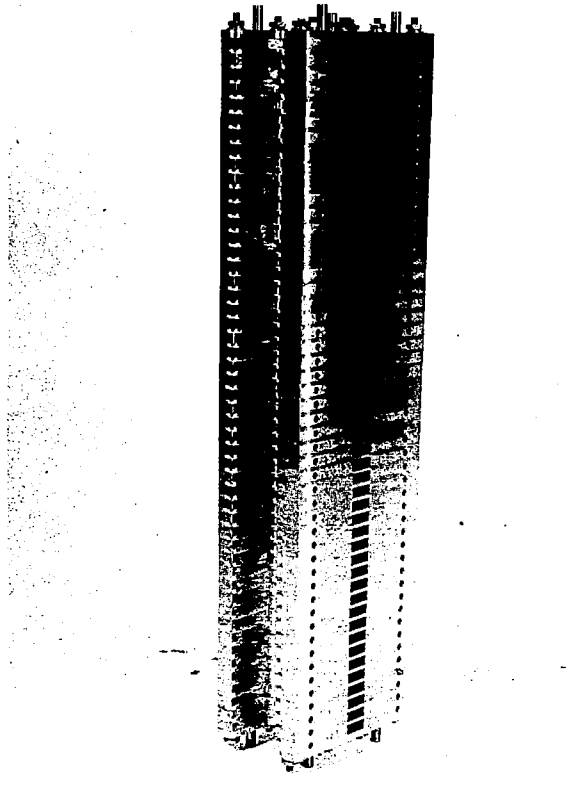

Figure 3. Phasing Section

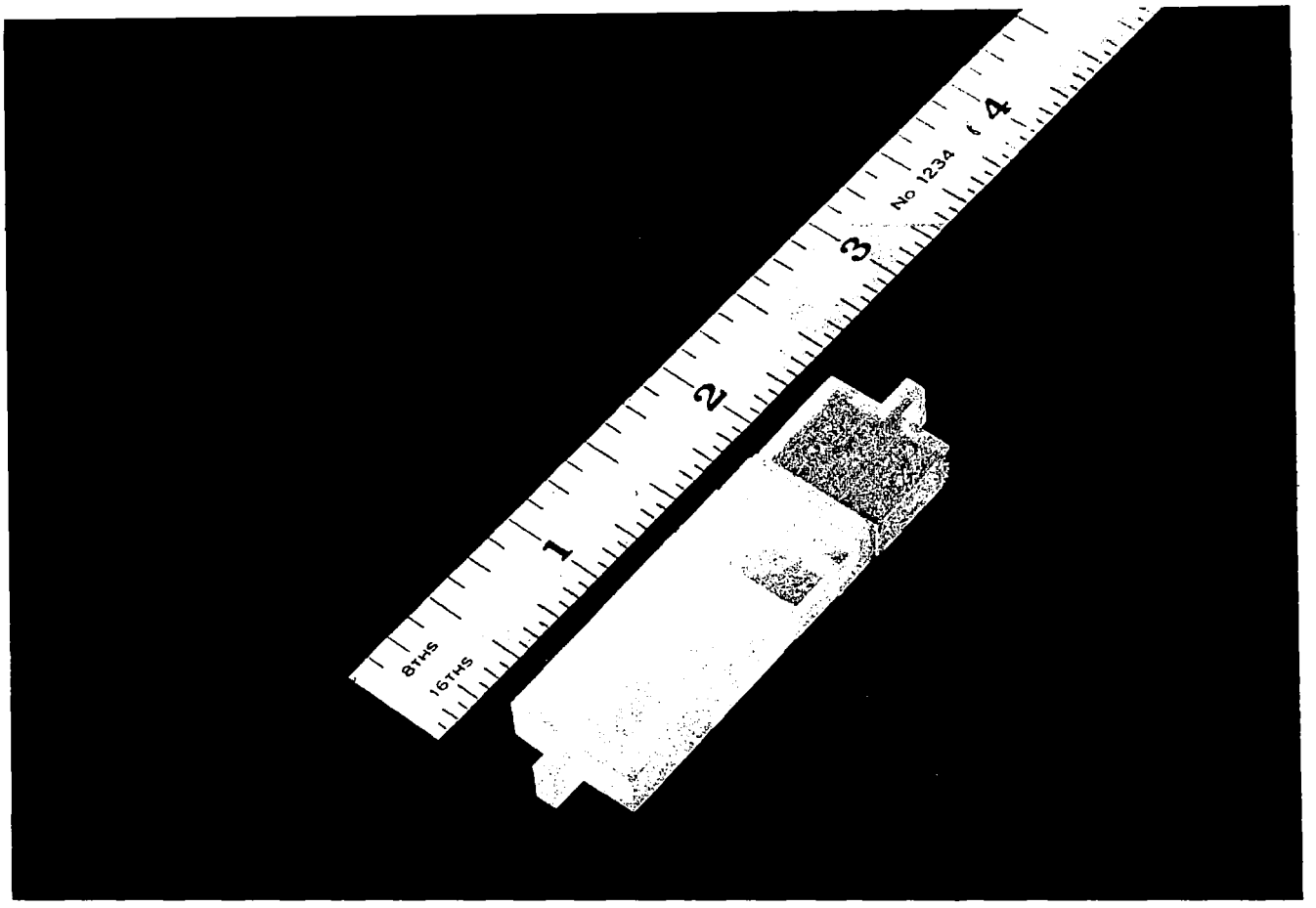

Figure 4. Five-Bit Phase Shifter

Fifty-Element Array

The array consists of 50 lens-compensated H-plane sectoral horns and is shown in Figure 5. The extremely low H-plane sidelobe characteristics of this element and the ability to reduce its E-plane dimension to restrict inter-element spacing and prevent grating lobe formation for the $\pm 60^{o}$ beam steering requirement resulted in its choice (Ref. 2).

The H-plane sectoral horn line source element is a dominant mode device. It derives its low sidelobe characteristics from the inherent H-plane distribution of the H_{10} mode modified by the dielectric lens structure (Ref. 6). The resultant output amplitude distribution of the lens-compensated H-plane sectoral horn, when a proper impedance match is obtained, is similar to a $\cos^2$ or $\cos^3$ distribution with resultant maximum antenna pattern sidelobes in the −32 to −40 dB range.

Inter-element spacing for the array is selected to be $\lambda/2$ at 16.8 GHz. This choice insures no grating lobe formation in visible space for the $\pm 60^{o}$ scan requirement and operating frequencies in the 15.2 to 16.8 GHz band.

The element dielectric lens is fabricated from Emerson-Cuming Stycast 0005, and employs impedance matching transformer sections on both its input and output surfaces. The lens is shown in Figure 6.

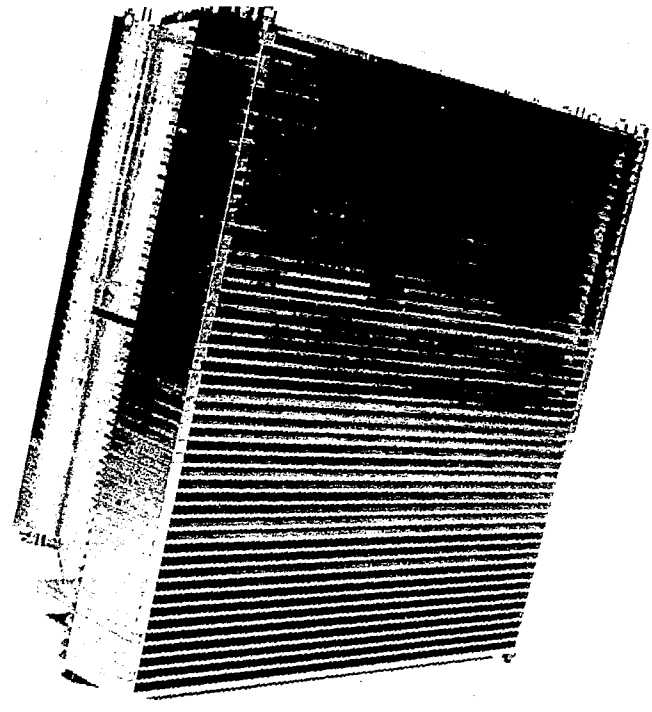

Figure 5(a). Fifty-Element Array Front View

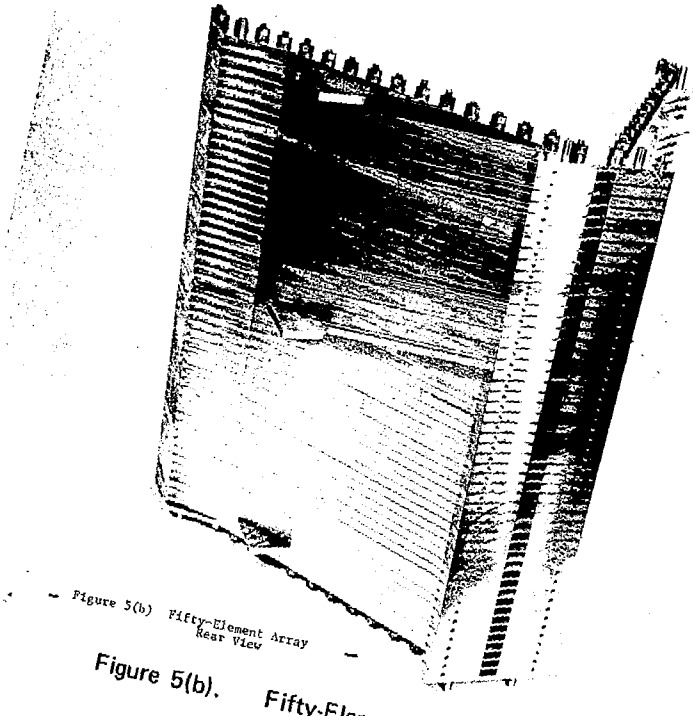

Figure 5(b) Fifty-Element Array Rear View

Figure 5(b). Fifty-Element Array Rear View

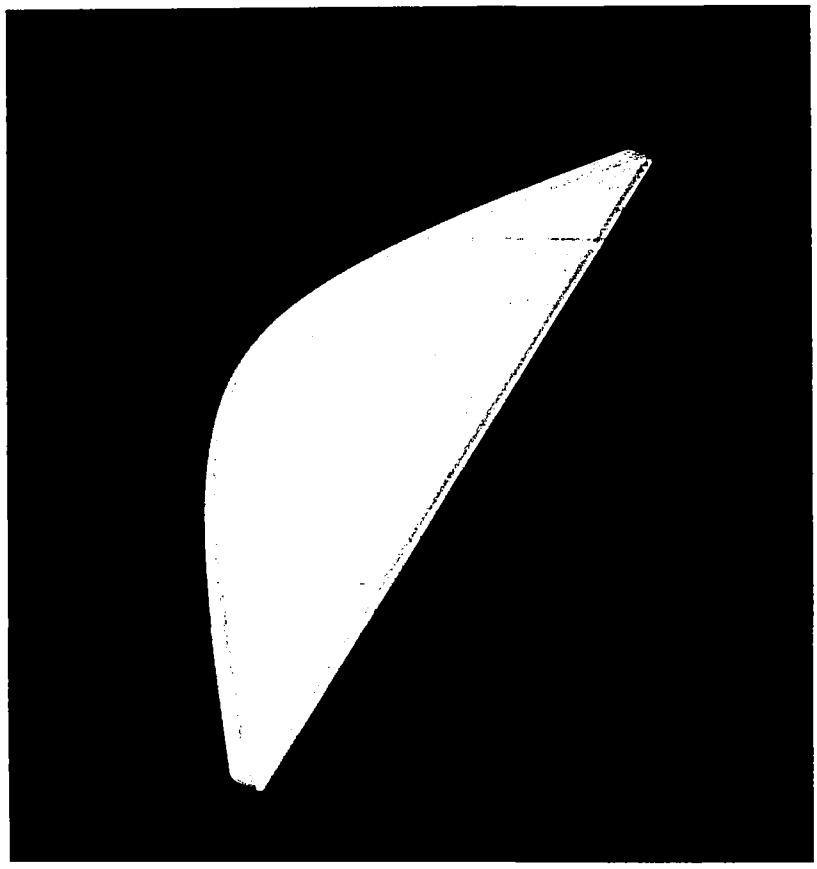

Figure 6. Array Element Lens

ARRAY EVALUATION

The experimental program undertaken to evaluate array performance began with determination of the individual phase shifter characteristics. When it was observed that phase shifter errors were slight, array pattern data was obtained for 0^{o}, 20^{o}, 40^{o}, and 60^{o} scan angles at several frequencies in the 15.2 to 16.8 GHz band. Beam efficiency was determined for several cases from the measured pattern data, and array gain and impedance characteristics were measured.

Phase Shifter Measurements

Phase shift data was obtained at mid-band for each bit and impedance transformer pair of the 50 dielectric 5-bit phase shifters. The short circuited waveguide-slotted line method described in Montgomery (Ref. 7) was used to obtain the data. The standard deviation of all the phase errors associated with the dielectric phase shifters was determined and is given in Table 1. From this data it is evident that the phase shifter elements are reasonably consistent.

The effect of the observed phase shifter errors on the array patterns was expected to be slight based on the data in Table 1 and on the analysis of pattern deterioration due to phase shifter errors by Yorinks (Ref. 3). Array pattern measurements, which will be discussed later, verified this fact.

TABLE I. STANDARD DEVIATION OF PHASE SHIFTER ERRORS MEASURED AT 16.0 GHz

Error Contribution	Standard Deviation
Insertion Phase	1.49^{o}
Bit Setting	
180^{o} Bit	0.66^{o}
90^{o} Bit	0.27^{o}
45^{o} Bit	0.64^{o}
22.5^{o} Bit	0^{o}
11.25^{o} Bit	1.06^{o}
Composite Bit Setting	1.01^{o}
Phase Shifter	1.80^{o}
	(0.031 radians)

Element Patterns

Radiation patterns of the individual H-plane sectoral horn array elements were taken to both explore for any indications of array resonance and to determine the basic element pattern characteristics as a function of location in the 50-element array.

E-plane patterns of several elements are shown in Figure 7 at the design frequency 16.0 GHz. It can be seen from this data that the pattern of the centrally located element possesses excellent symmetry and is free from rapid amplitude oscillations over a $\pm 90^{o}$ region. Elements located at and near the edge display the assymetries expected from edge effects with some increasing amplitude oscillation as the element location approaches the array edge.

Element patterns at other frequencies in the 15.2 to 16.8 GHz band have similar characteristics as seen from Figure 8.

Element H-plane patterns are shown in Figure 9 for several frequencies and element locations. As observed previously (Ref. 2), the H-plane patterns are characterized by extremely low sidelobes and are relatively insensitive to location within the array.

Principal Plane Array Patterns

Phase shifter combinations required to scan the array beam to 20^{o}, 40^{o}, and 60^{o} in the E-plane were determined for operation at 16.0 GHz. E- and H-plane array patterns were then obtained over the 15.2 to 16.8 GHz frequency band for the above combinations and for the broadside case with all phase shifters removed.

As a result of the phase shifter settings, the beam scans to the designated angles at only the design frequency. Since the phase shift associated with the dielectric phase shifters is inversely proportional to frequency, the designated phase shifter settings will produce greater scan at frequencies below the design frequency and reduced scan at higher frequencies. This effect can be observed in the measured pattern data that follows.

E-plane broadside and scanned patterns at 16.0 GHz are shown in Figure 10. Maximum sidelobe level increases from −28 dB to −18 dB as the array beam is scanned from 0^{o} to 60^{o}. The maximum sidelobe at 40^{o} scan is only slightly greater than −25 dB. Scanned pattern data at other frequencies is shown in Figure 11.

H-plane patterns obtained at 16.0 GHz, for the 0^{o}, 20^{o}, 40^{o}, and 60^{o} E-plane scanned cases, are shown in Figure 12. These patterns are characterized by maximum sidelobe levels which in most cases only slightly exceed −40 dB. H-plane pattern data at other frequencies exhibited similar characteristics and are shown in Figure 13.

Array Pattern Contours

Field amplitude contours were obtained for the full array at broadside and with the beam steered to 20^{o}, 40^{o}, and 60^{o} in the E-plane. Contour data is plotted in Figure 14 for mid-band operation. The contour levels and peak values are indicated in dB. It can be seen from this data that the predominant sidelobes exist in the E-plane and, except for the 60^{o} scan case, all remaining sidelobes throughout the radiation sphere do not exceed −40 dB. This data indicates that beam efficiency will be extremely high because of the apparent lack of appreciable sidelobes throughout the radiation sphere surrounding the array.

Contour data at other frequencies in the 15.2 to 16.8 GHz band is plotted in Figure 15. This data is similar to that obtained at mid-band except for the E-plane sidelobe levels which increase as frequency approaches the band edges.

Array Beam Efficiency

Beam efficiency of the low-sidelobe array has been determined as a function of scan angle and frequency using an integration technique similar to that described in Reference 2. Contour and principal plane patterns furnished the data required for the calculation. Pattern integrations were obtained for the principal, diagonal, 15^{o}, 30^{o}, 60^{o}, and 75^{o} radiation planes to insure accuracy.

Beam efficiency is plotted as a function of scan angle and frequency in Figure 16. As expected, it is maximum for broadside and deteriorates slowly as the beam is scanned. Beam efficiency ranges from 98.6 to 90% for 0^{o} to 40^{o} scan over the 15.2 to 16.8 GHz frequency band. With the beam steered to 60^{o}, beam efficiency falls off to values in the 85 to 77% range. Maximum beam efficiency of 98.6% occurs at 16.0 GHz for broadside operation.

Array Gain

Antenna gain was determined as a function of frequency and scan angle for the low-sidelobe array using a standard gain horn as a gain reference. Antenna gain is plotted versus frequency in Figure 17 for 0^{o}, 20^{o}, 40^{o}, and 60^{o} scan angles. The broadside gain at mid-band is 33.8 dB which corresponds to an antenna efficiency of approximately 34%.

The E- and H-plane aperture distributions of the low-sidelobe array can be approximated respectively by an almost completely tapered dual-mode distribution, which is a full-cycle cosine (Ref. 1), and a $\cos^{3}$ distribution. The line source efficiencies associated with these distributions are approximately 66% and 57%. The expected array aperture efficiency is the product of these, or 37.5%. The corresponding measured array aperture efficiency is 3.5% below this figure; hence the measured gain is approximately 0.4 dB less than that expected from a lossless antenna with the above distributions. The gain difference is partially attributable to measurement accuracy, slight array phase errors which occur as a result of fabrication tolerances, and array insertion loss.

Array and Element VSWR

The input VSWR of the complete low-sidelobe array was determined for the 0^{o}, 20^{o}, 40^{o}, and 60^{o} scan cases. VSWR versus scan angle at mid-band is plotted in Figure 18. VSWR versus scan angle is plotted for several other frequencies in Figure 19. The VSWR of the power combiner horn-phasing section combination, with all fifty ports terminated in matched loads, is plotted in Figure 20. This data is not significantly different from the array broadside VSWR implying that the array aperture is well matched and the resulting predominant reflection coefficient component is introduced by the power combiner. VSWR measurements of the power combiner horn filled with absorber material indicate that the primary contributor to array VSWR is the mode generating discontinuity and that the power combiner horn-phasing section interface is well matched. No attempt was made to match the mode generating discontinuity since its effect is not intolerable. This can be accomplished using reactive elements in the dominant mode region preceding the discontinuity.

Element VSWR data was obtained by measuring at a single input array port with waveguide loads in the remaining forty-nine ports. This data is plotted in Figure 21 for several edge and centrally located elements. It can be seen from this data that element VSWR is relatively insensitive to element location within the array.

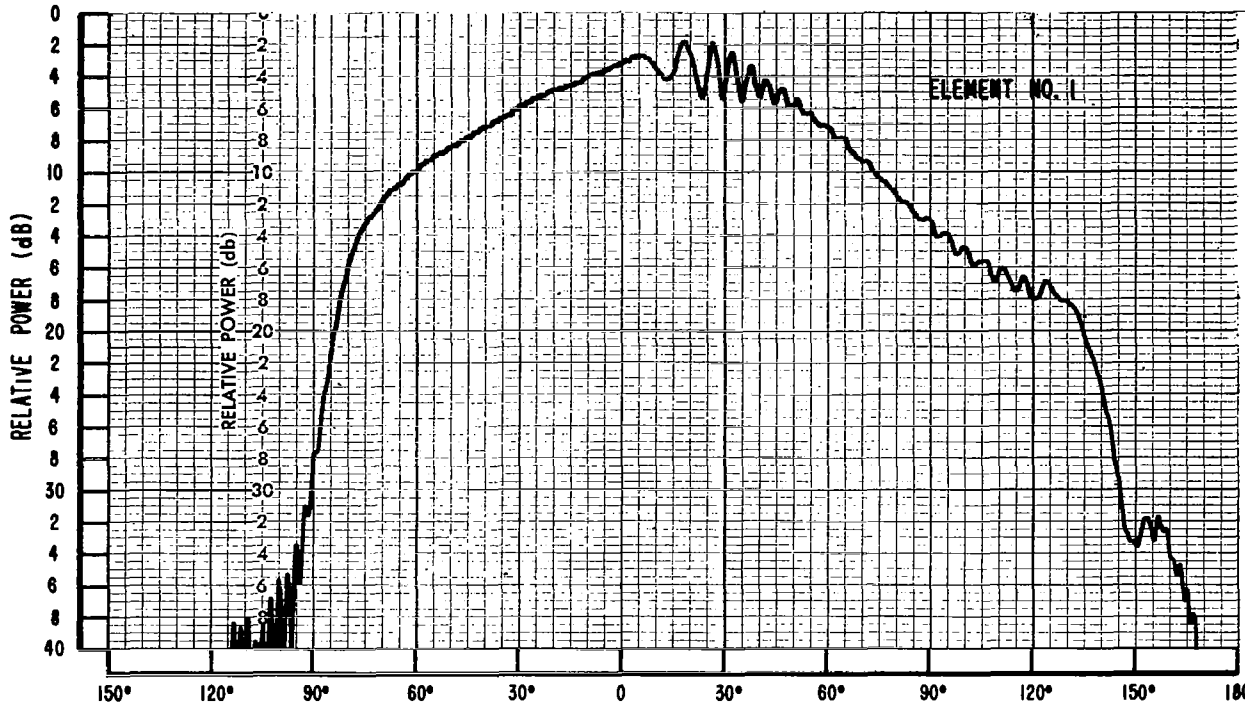

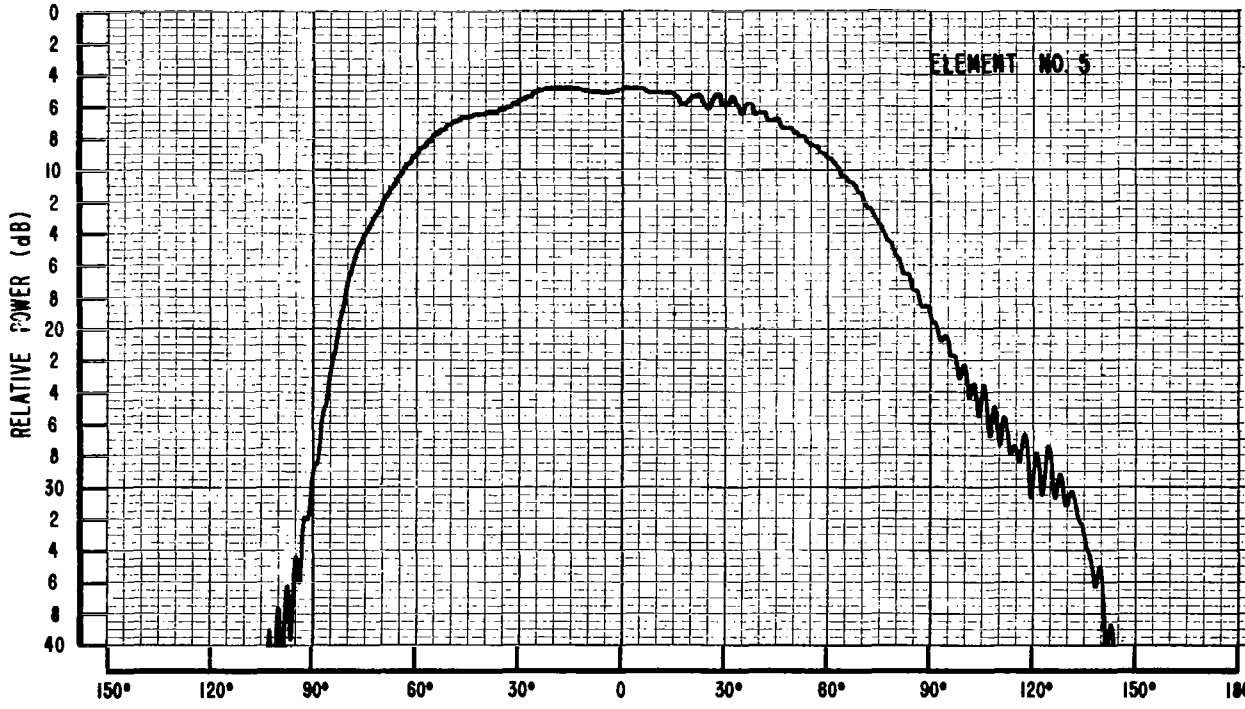

Figure 7(a). Element E-Plane Patterns - 16.0 GHz

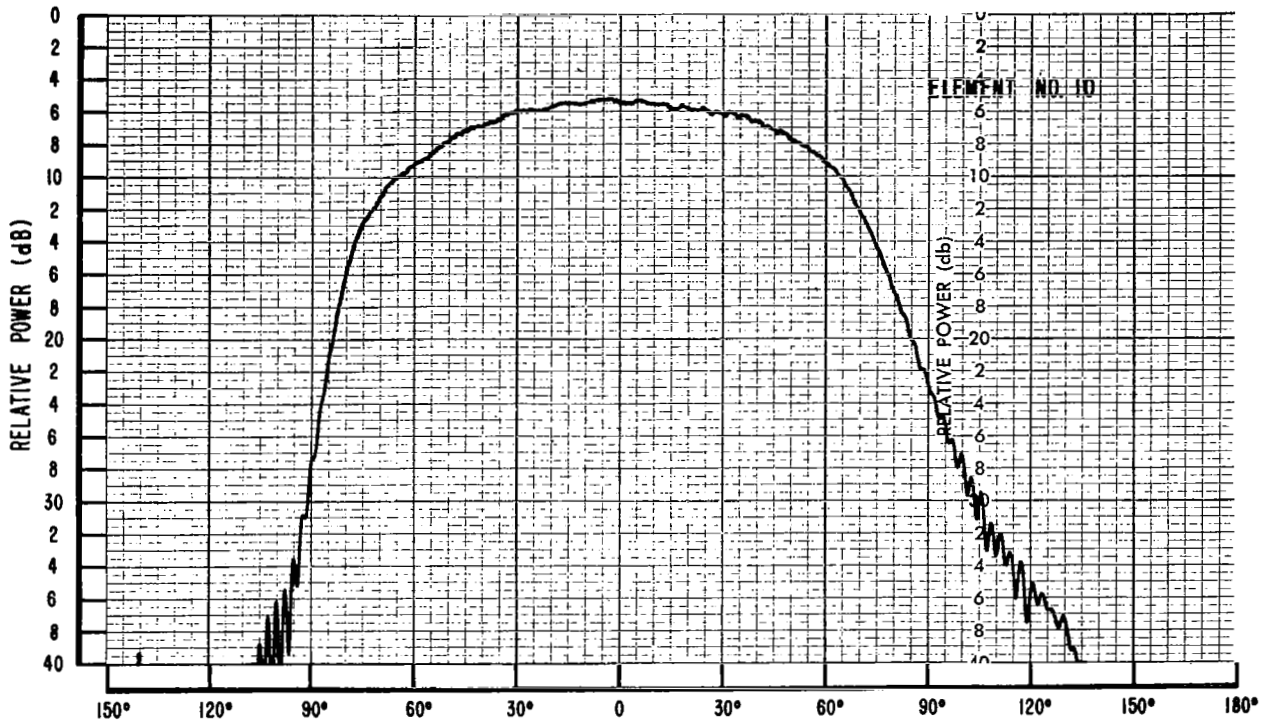

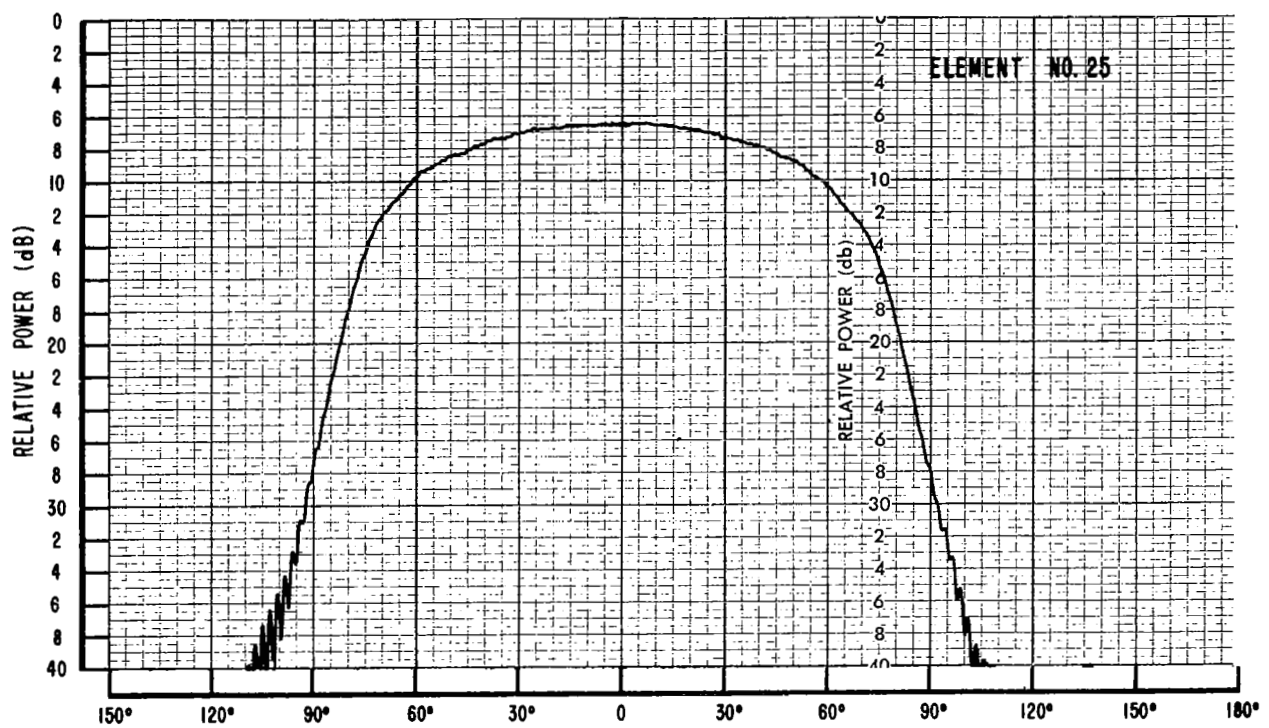

Figure 7(b). Element E-Plane Patterns - 16.0 GHz

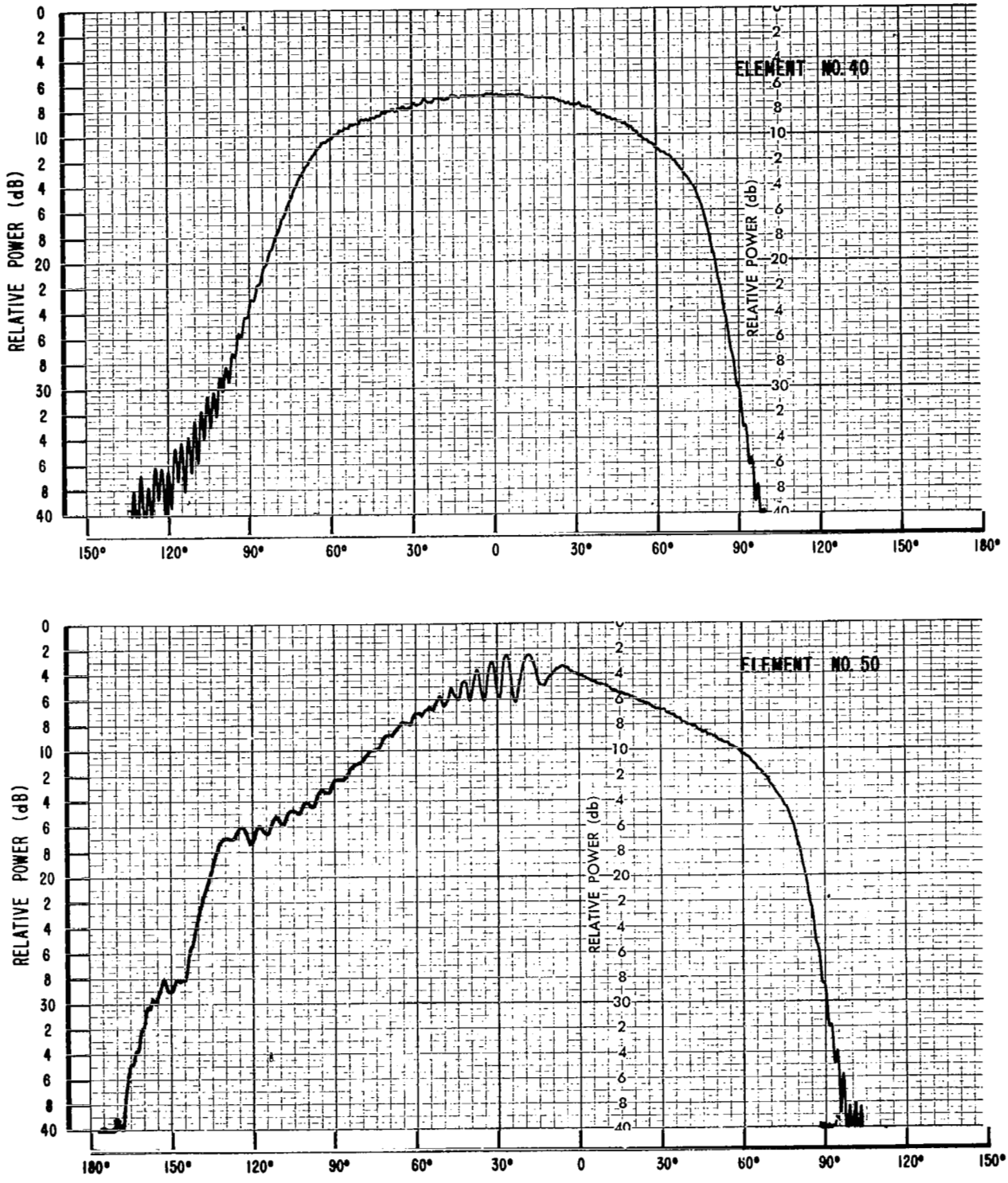

Figure 7(c). Element E-Plane Patterns - 16.0 GHz

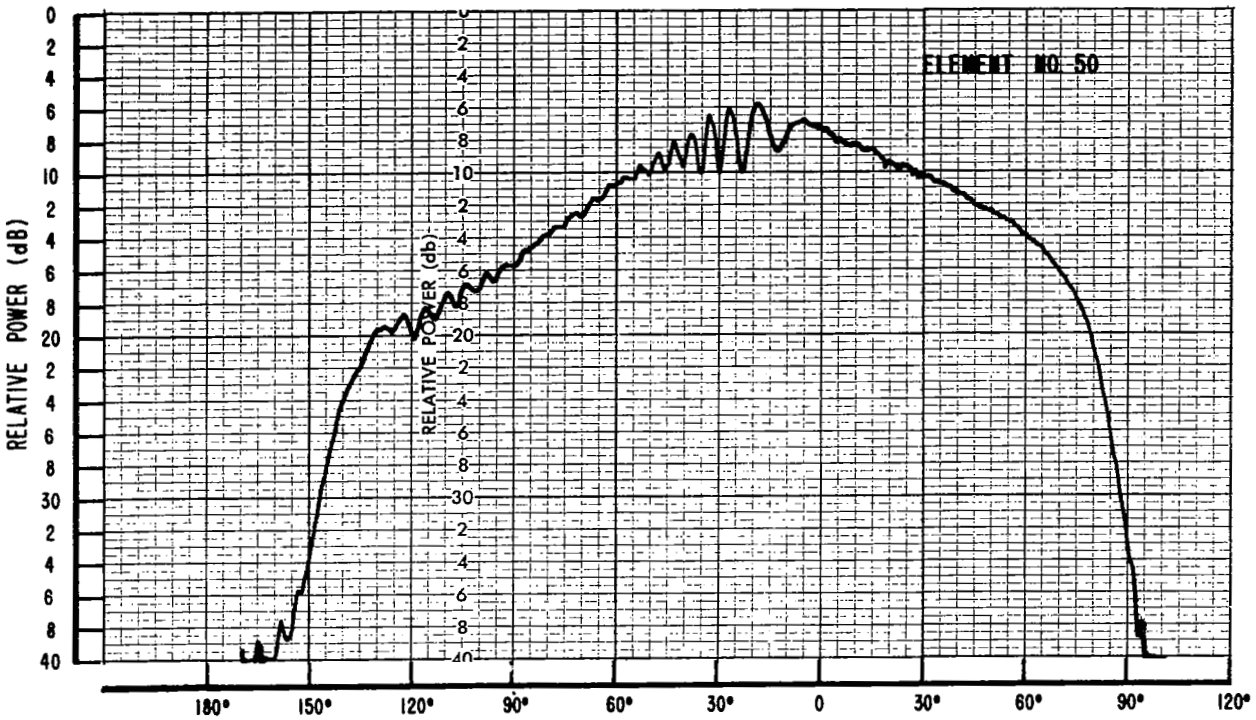

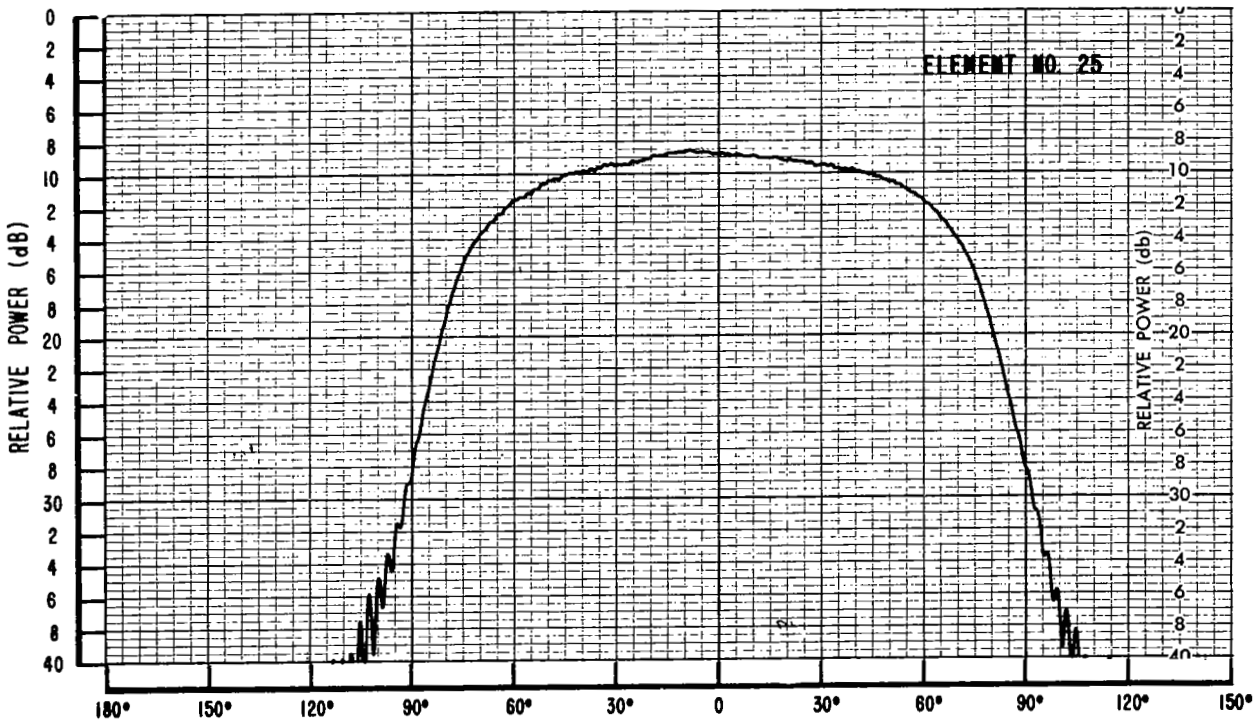

Figure 8(a). Element E-Plane Patterns - 15.2 GHz

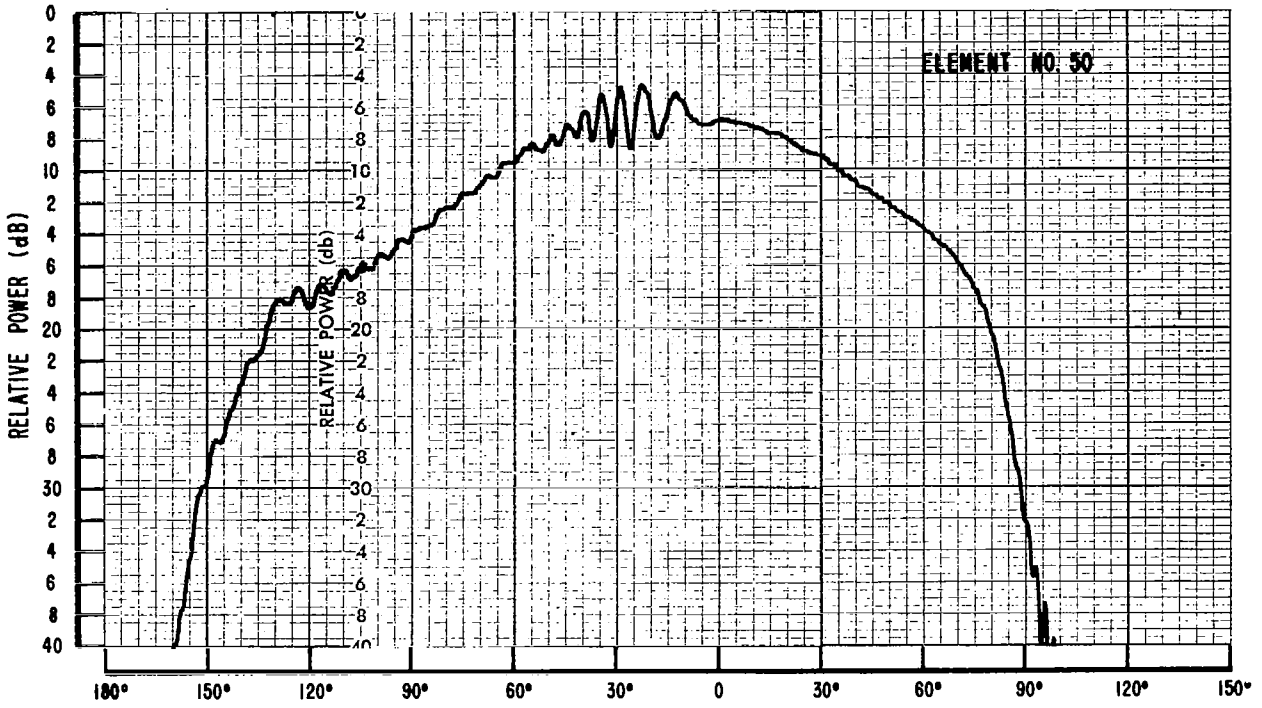

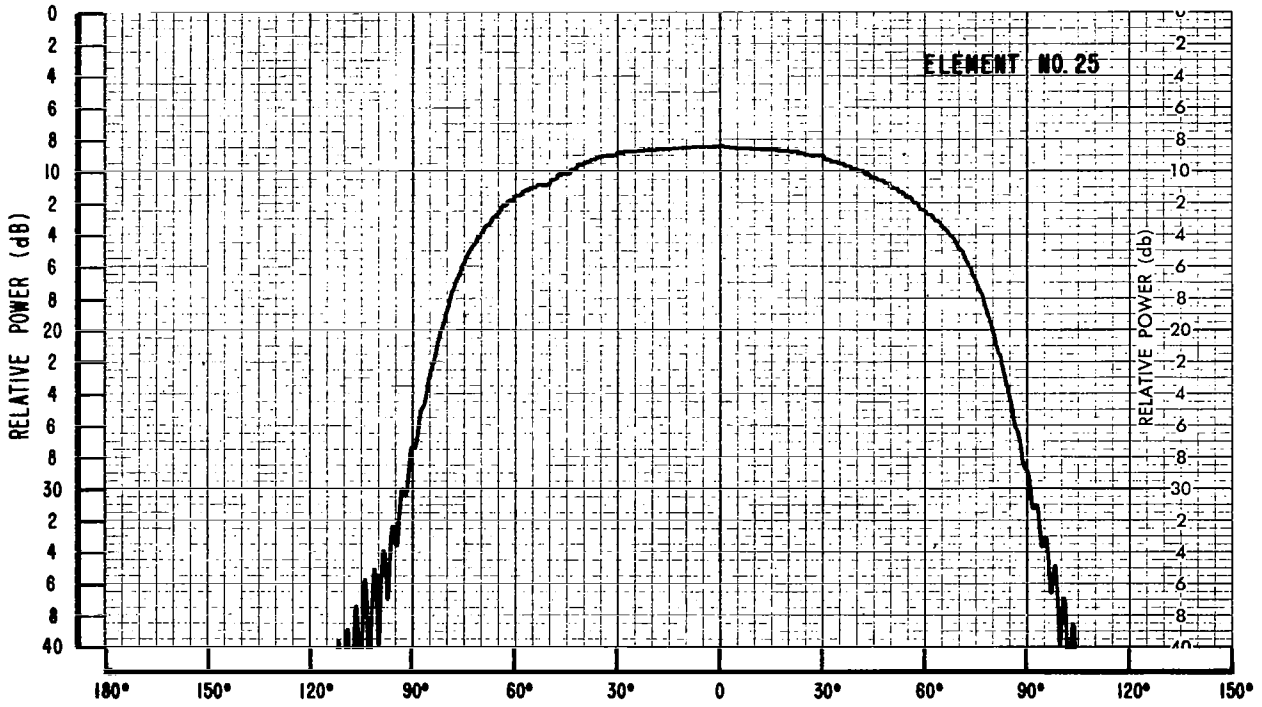

Figure 8(b). Element E-Plane Patterns - 15.6 GHz

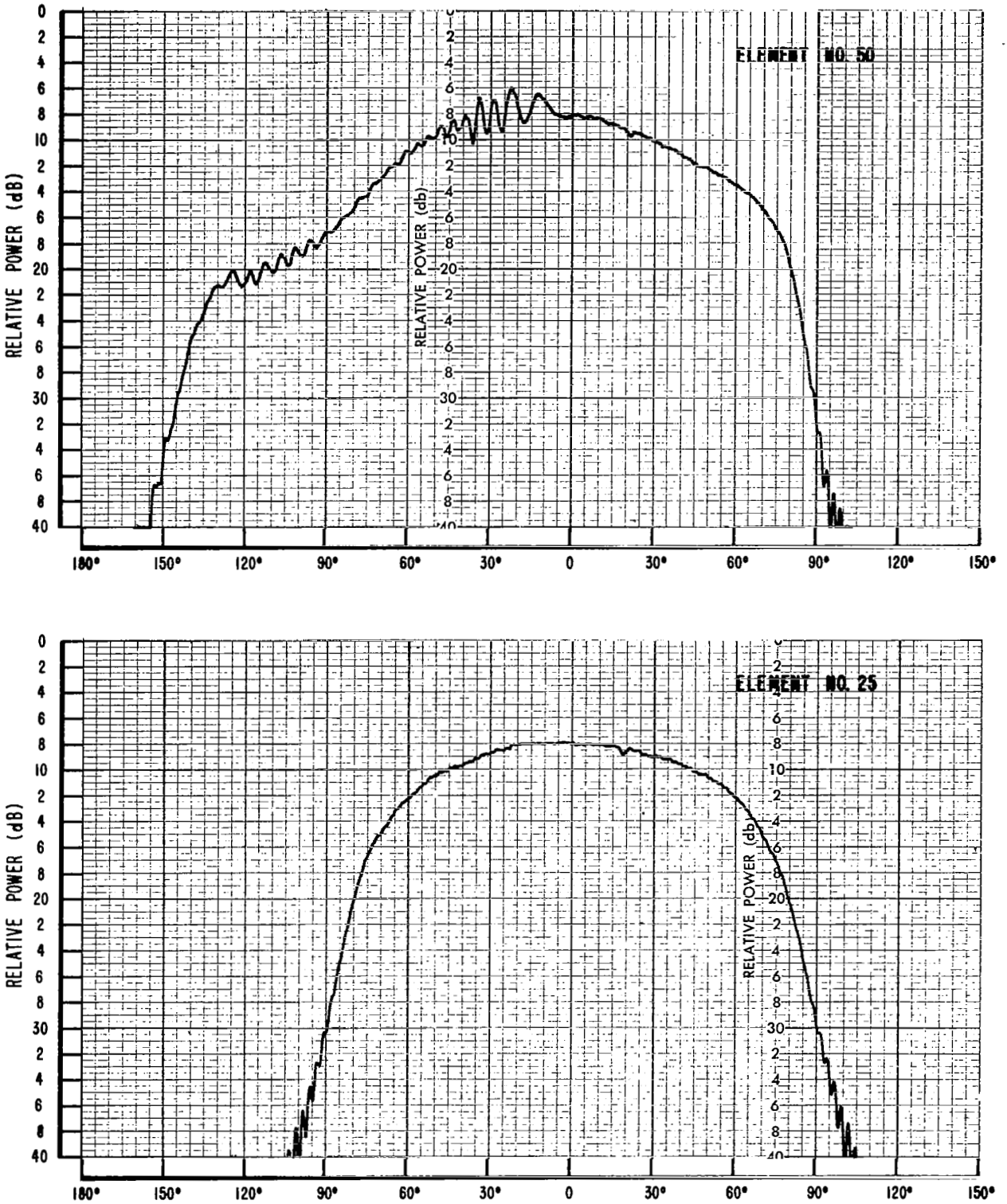

Figure 8(c). Element E-Plane Patterns - 16.4 GHz

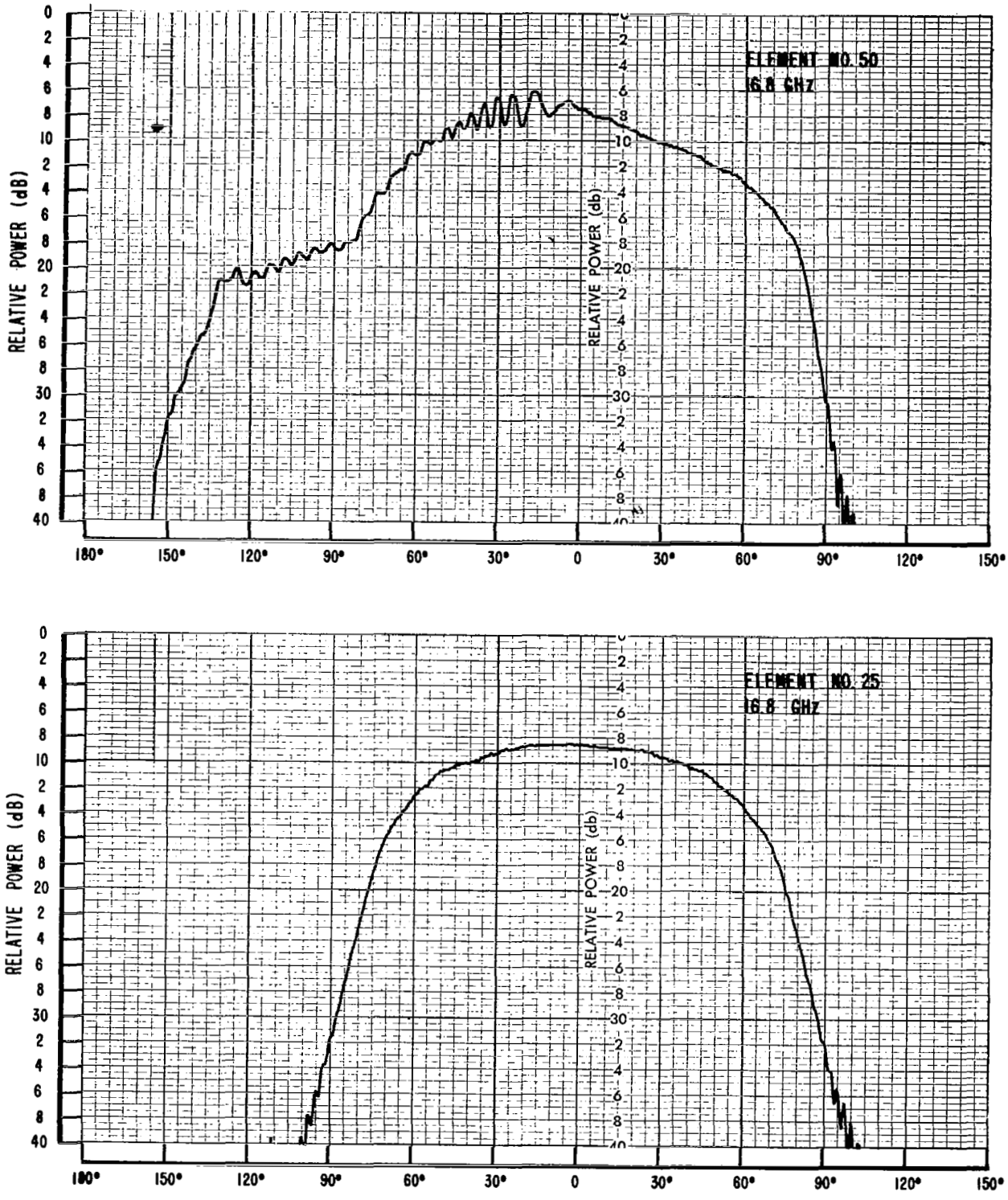

Figure 8(d). Element E-Plane Patterns - 16.8 GHz

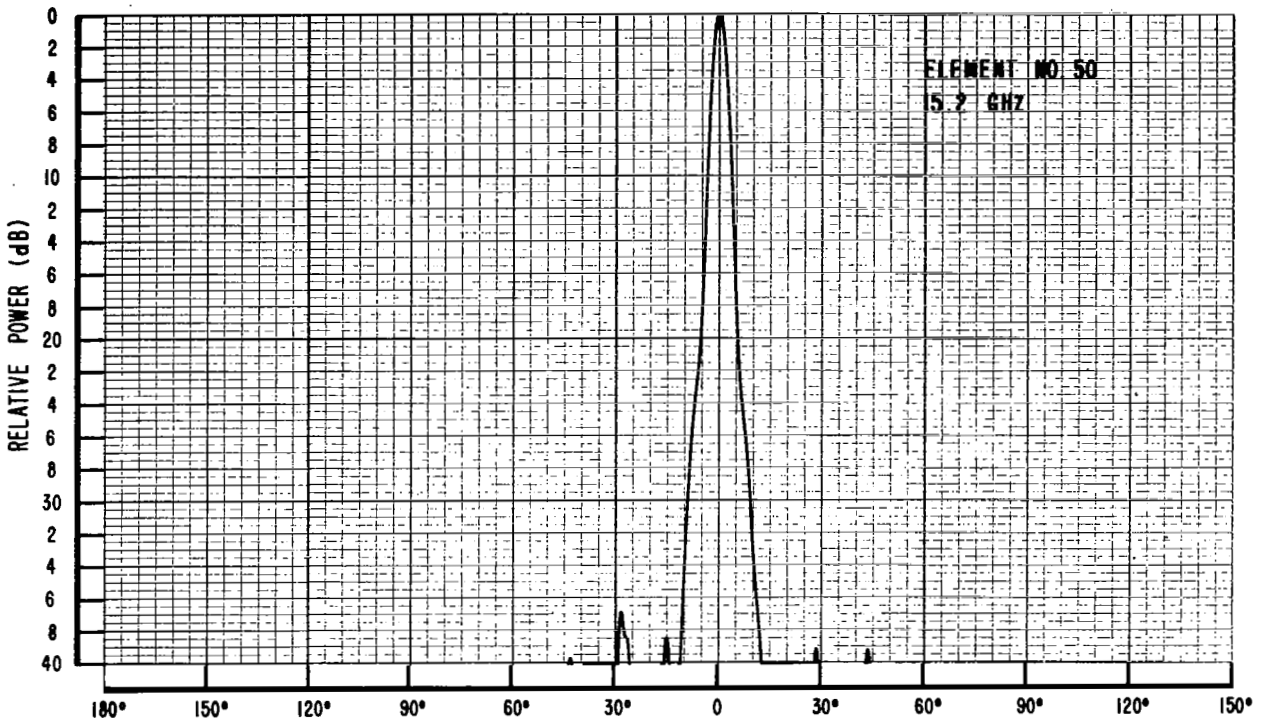

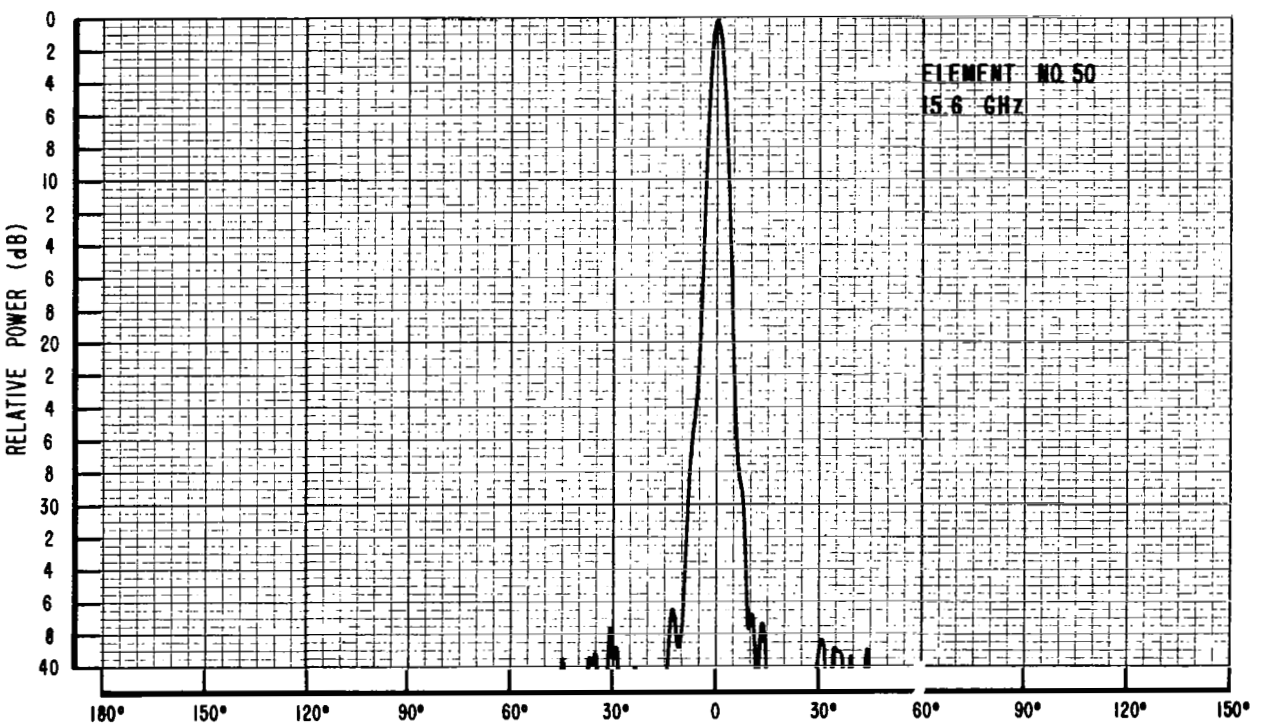

Figure 9(a). Element H-Plane Patterns

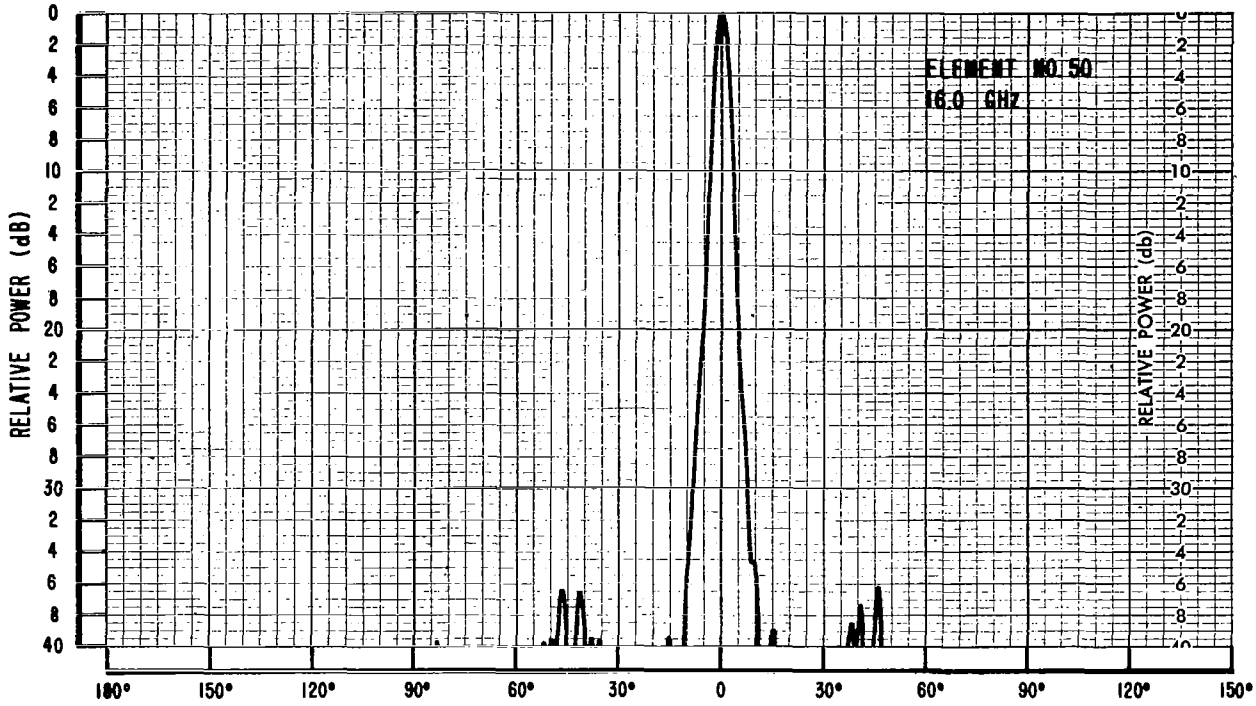

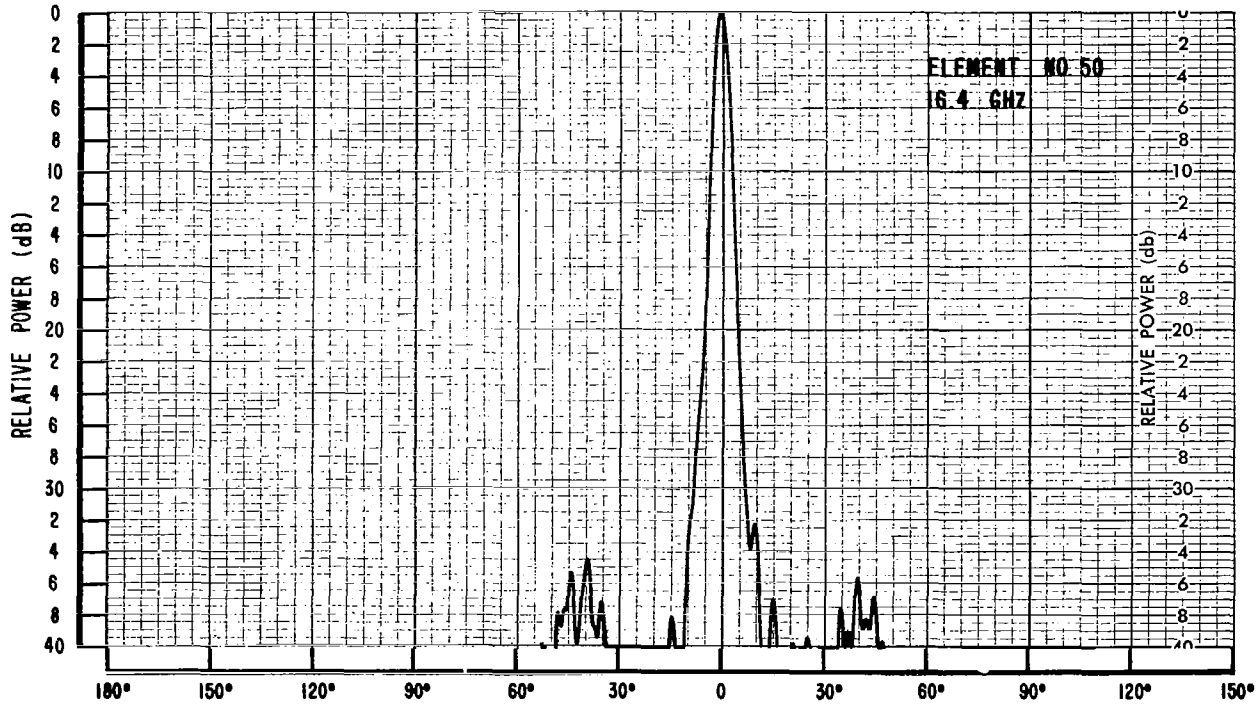

Figure 9(b). Element H-Plane Patterns

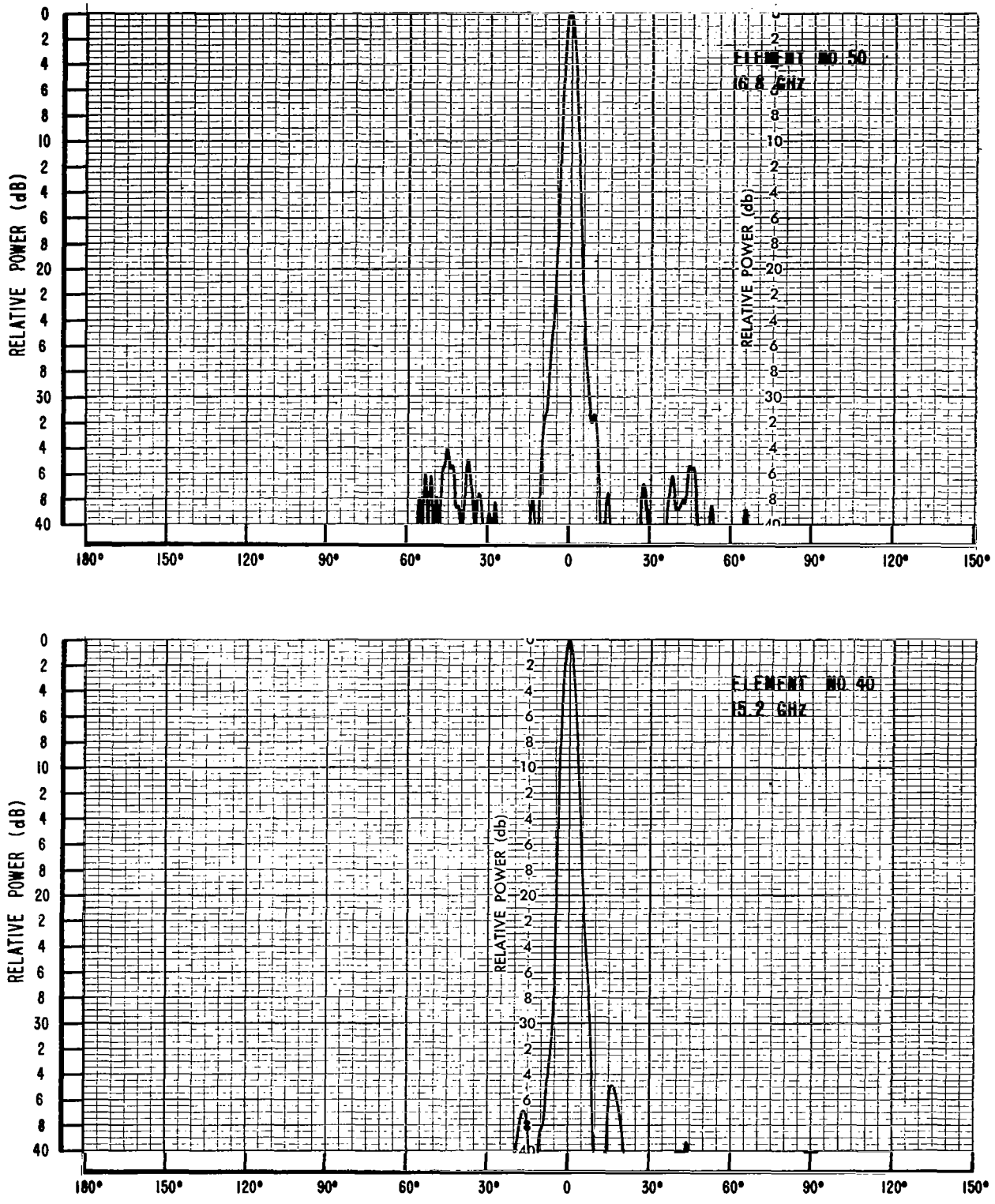

Figure 9(c). Element H-Plane Patterns

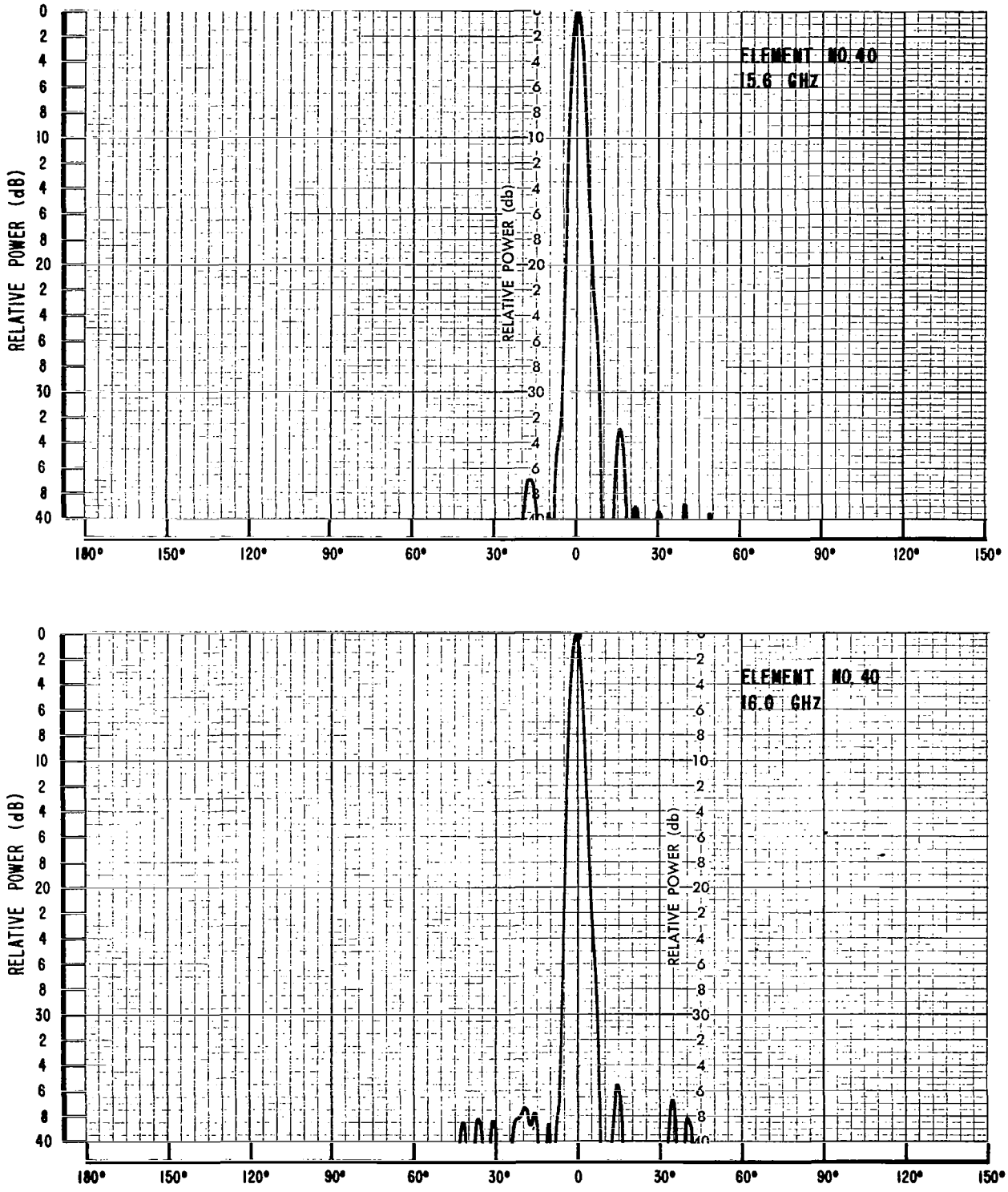

Figure 9(d). Element H-Plane Patterns

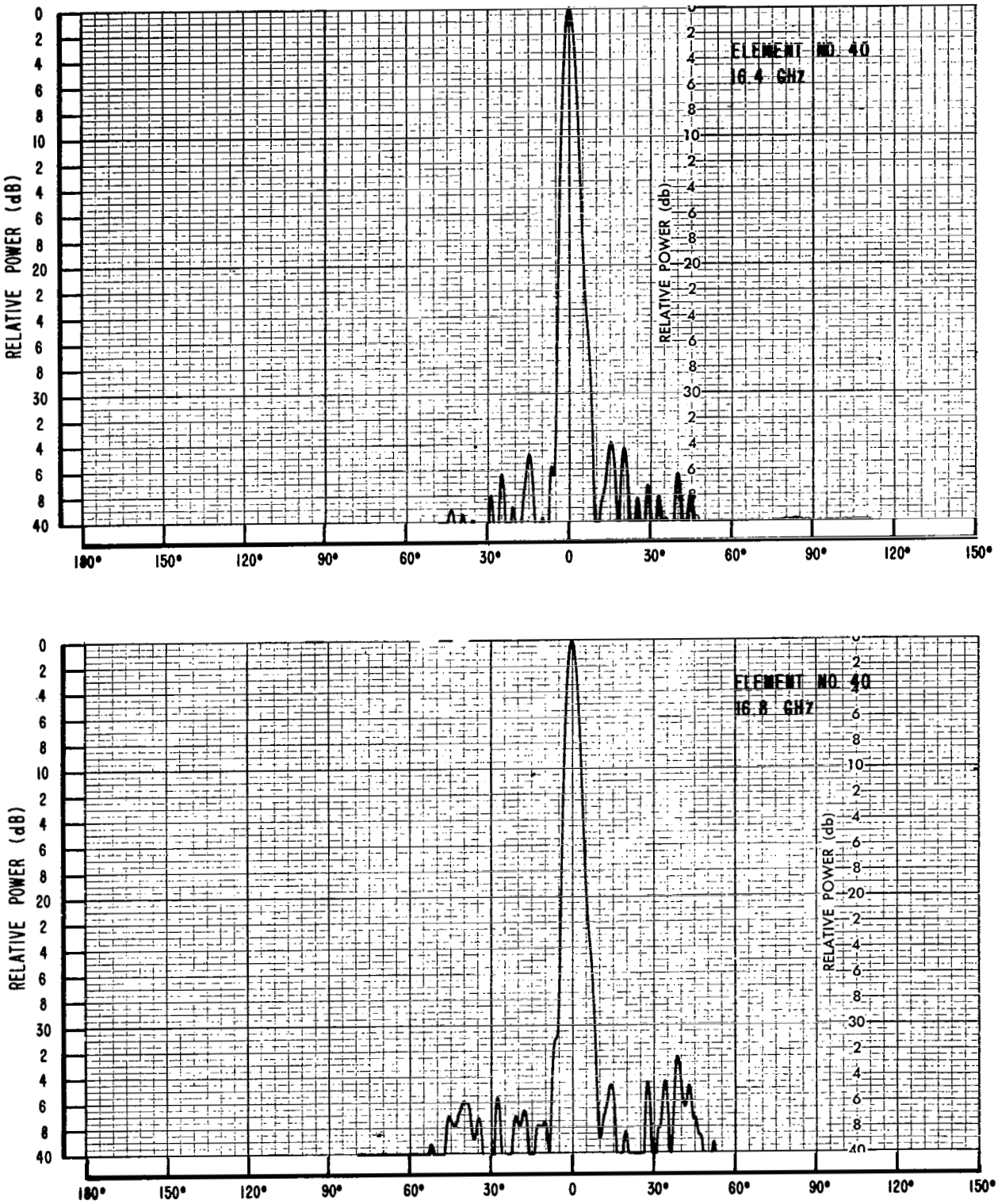

Figure 9(e). Element H-Plane Patterns

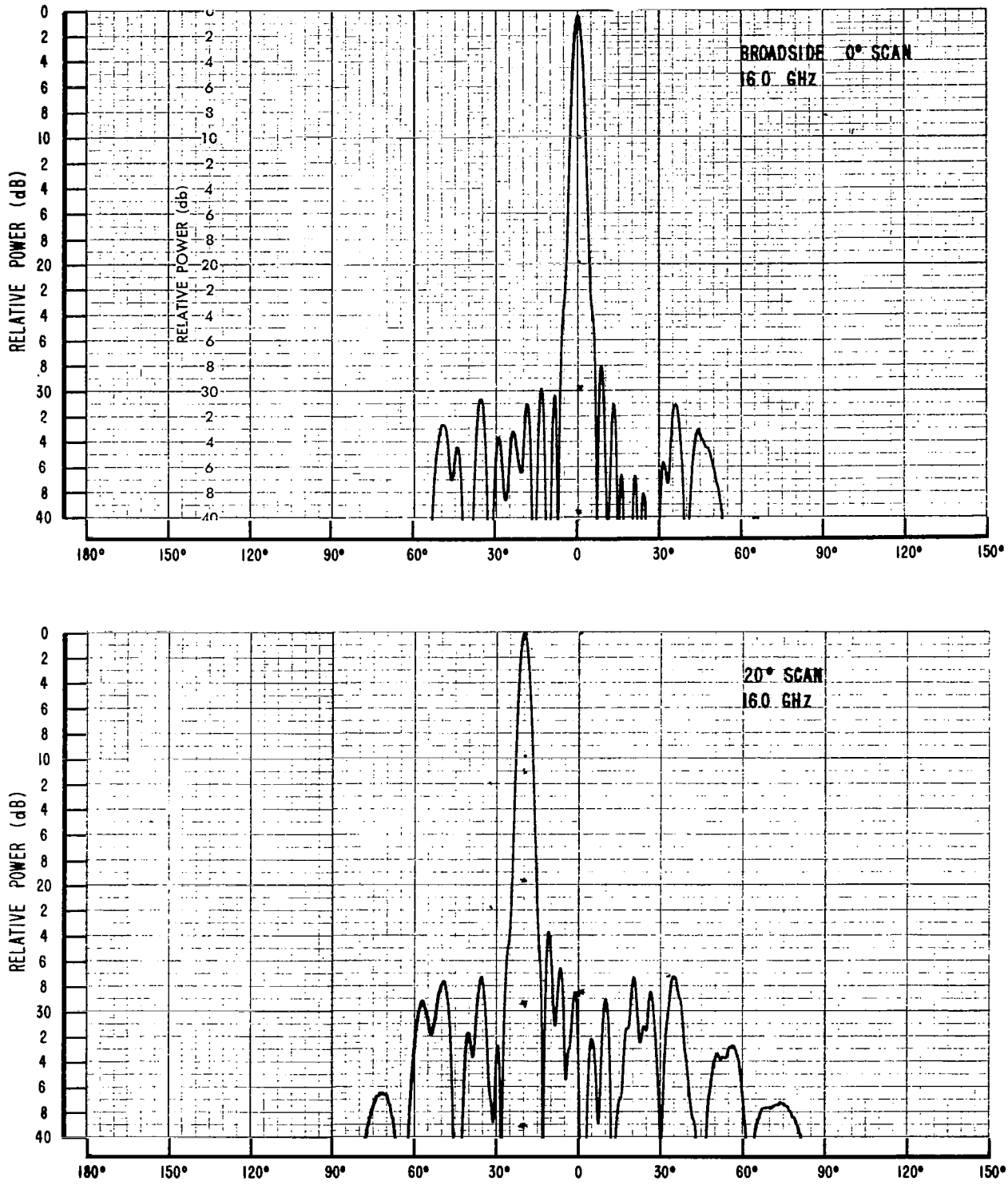

Figure 10(a). Array E-Plane Patterns - 16.0 GHz

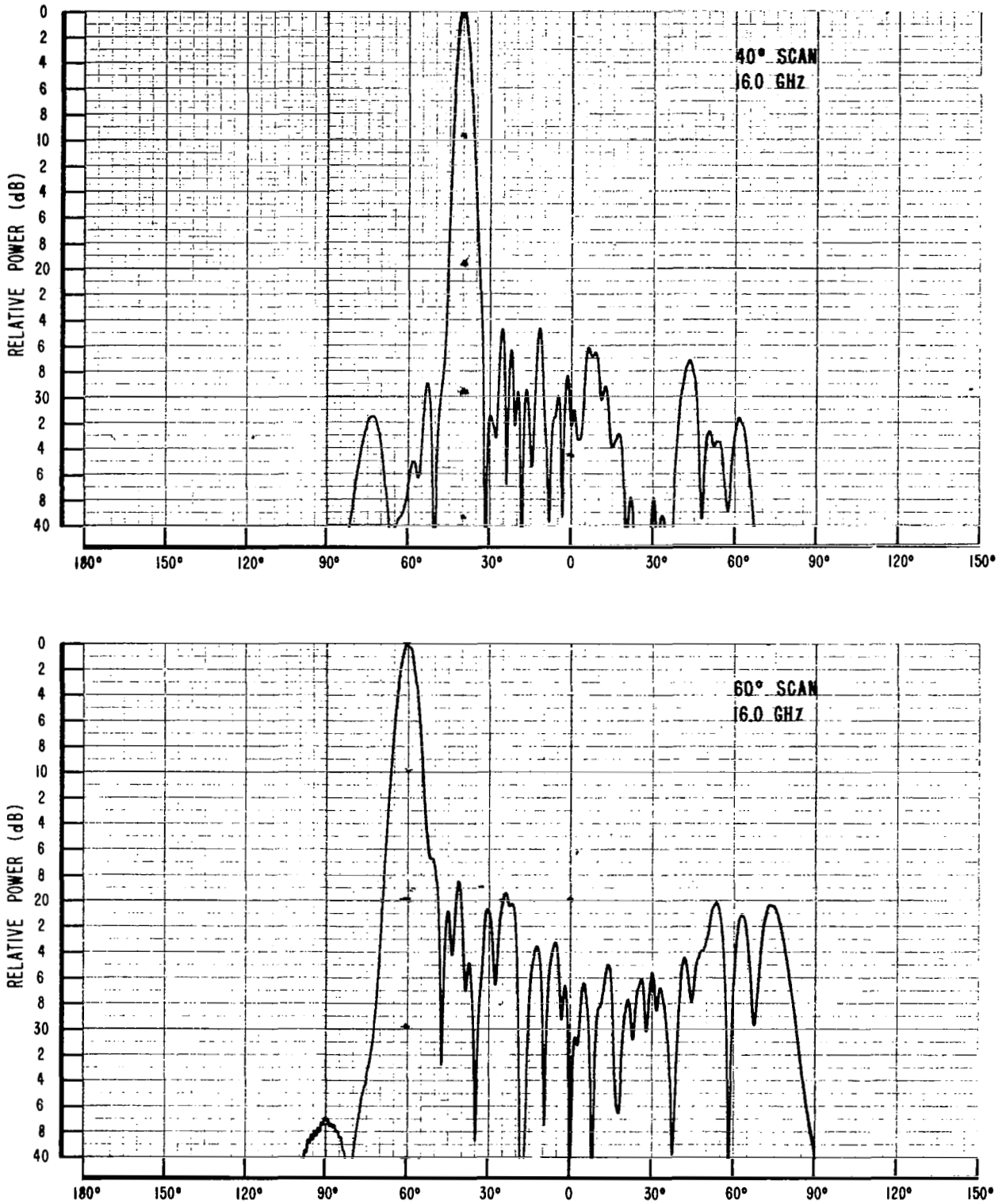

Figure 10(b). Array E-Plane Patterns - 16.0 GHz

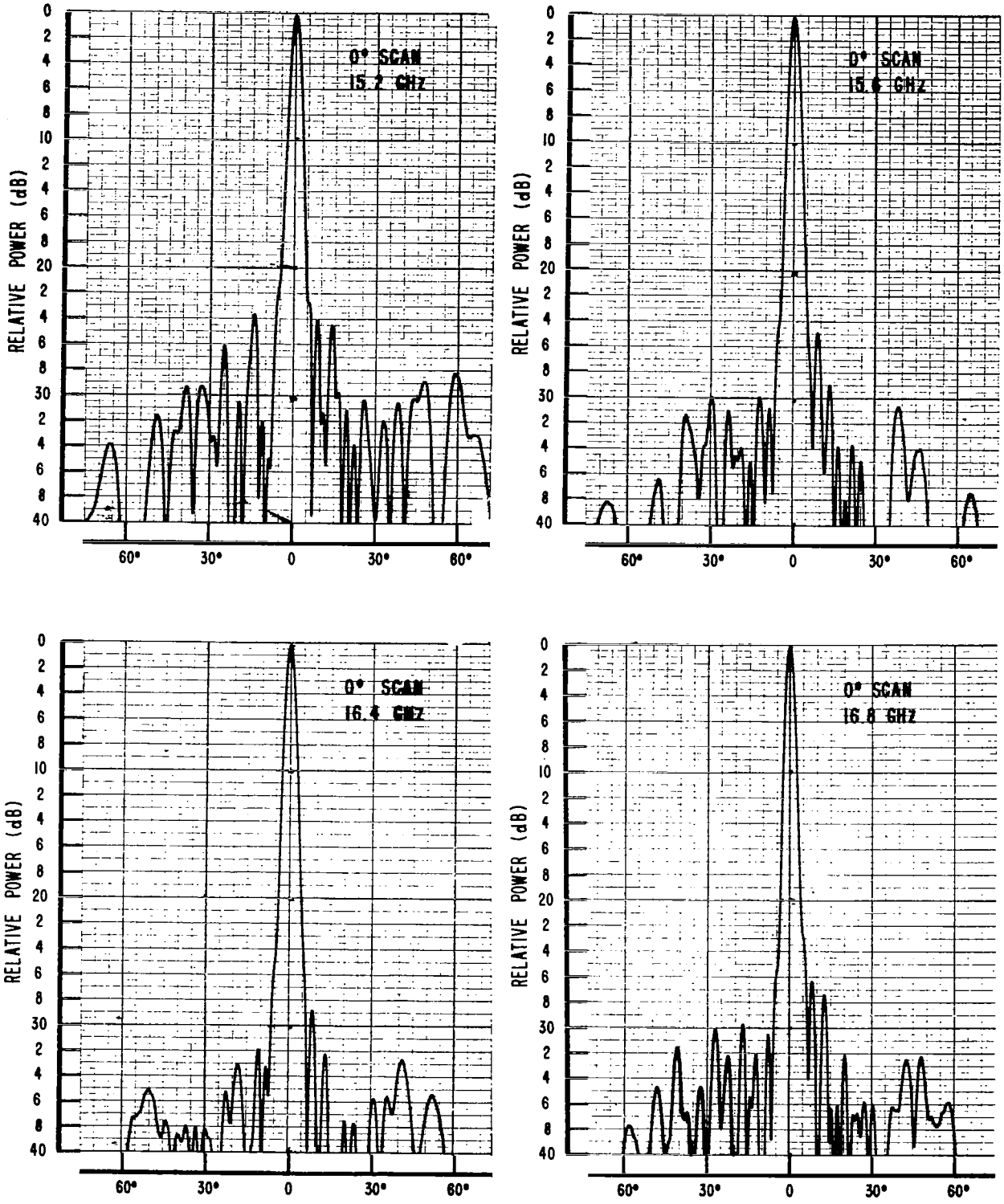

Figure 11(a). Array E-Plane Patterns - 0^{o} Scan

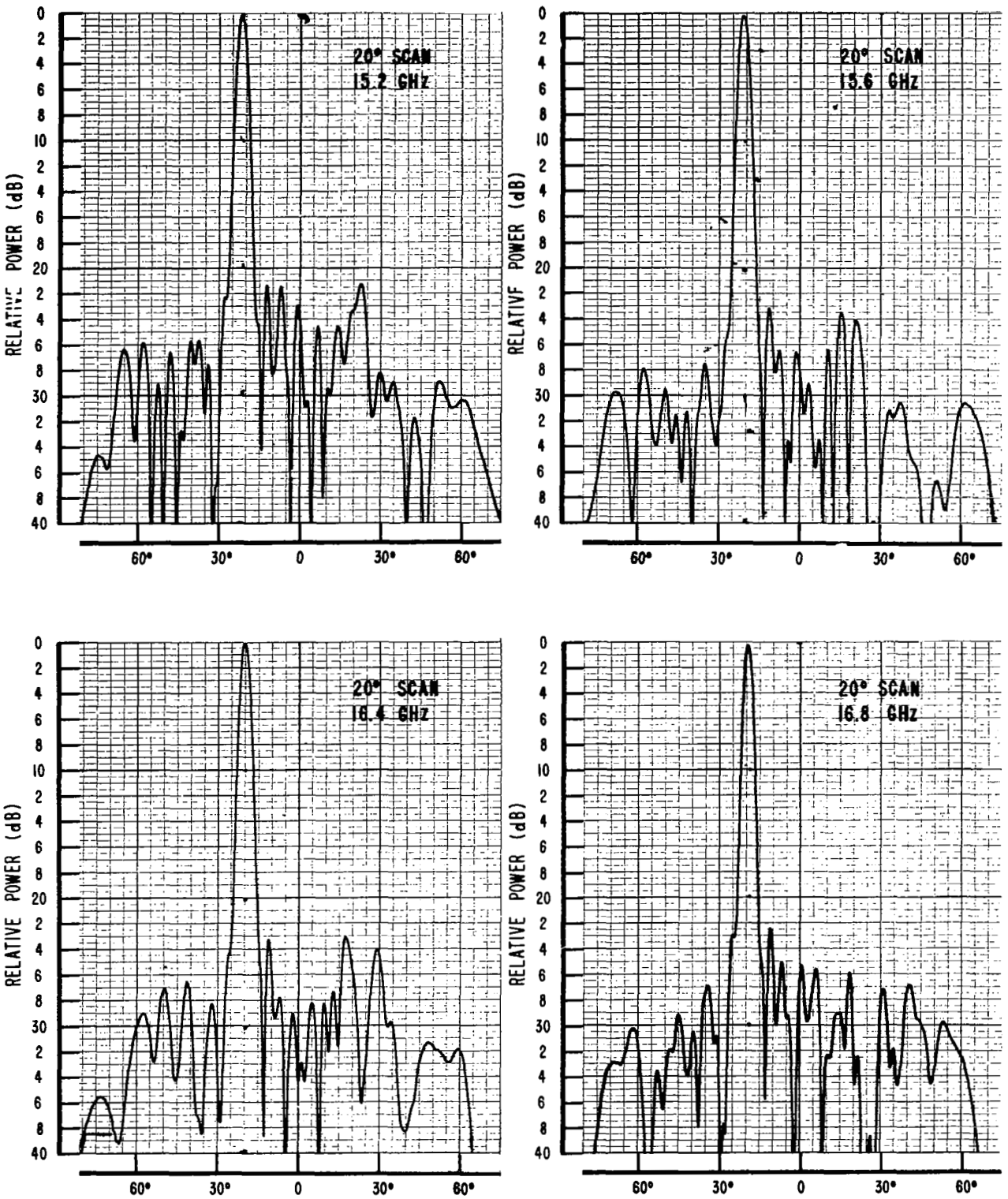

Figure 11(b). Array E-Plane Patterns - 20° Scan

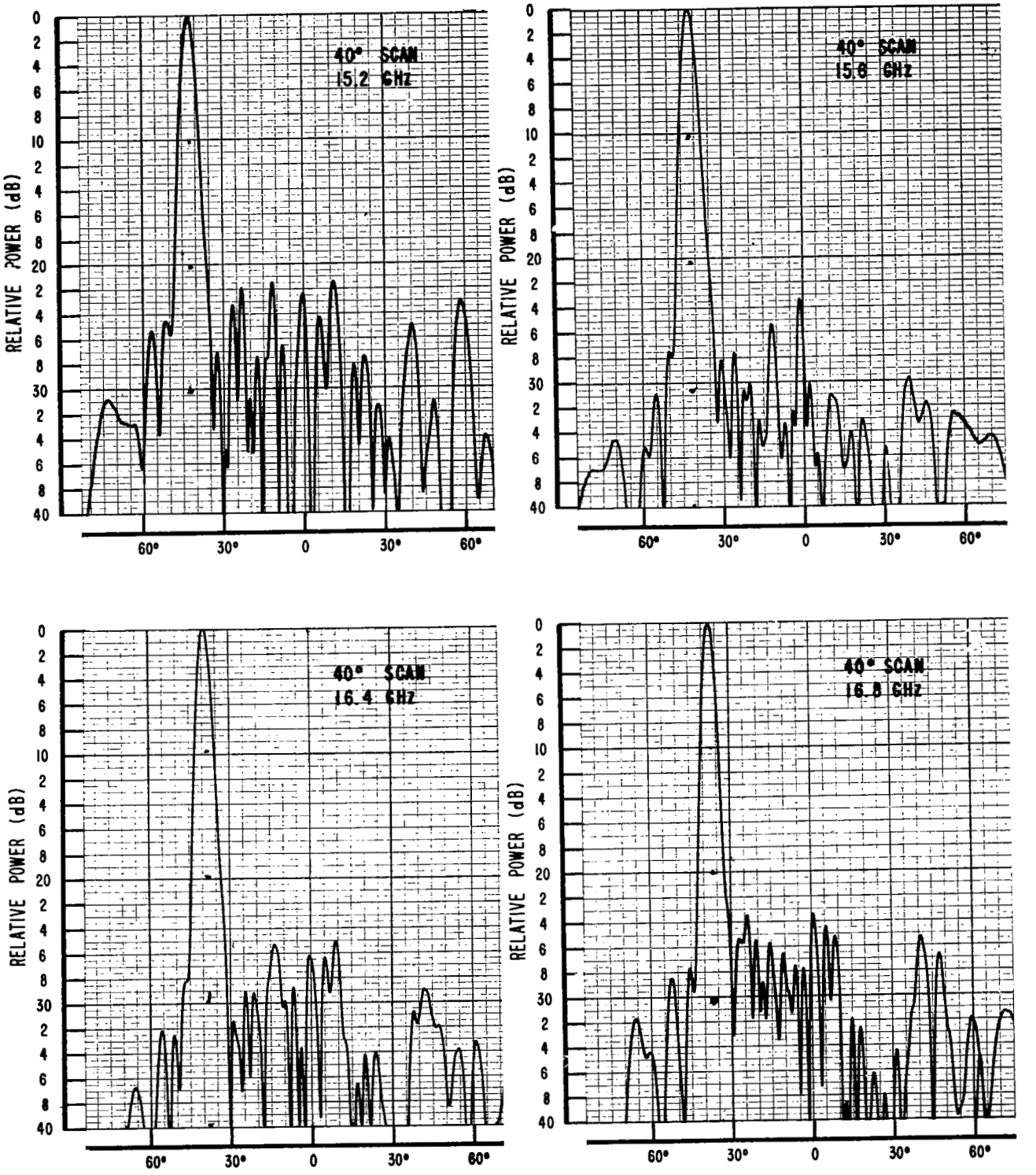

Figure 11(c). Array E-Plane Patterns - 40° Scan

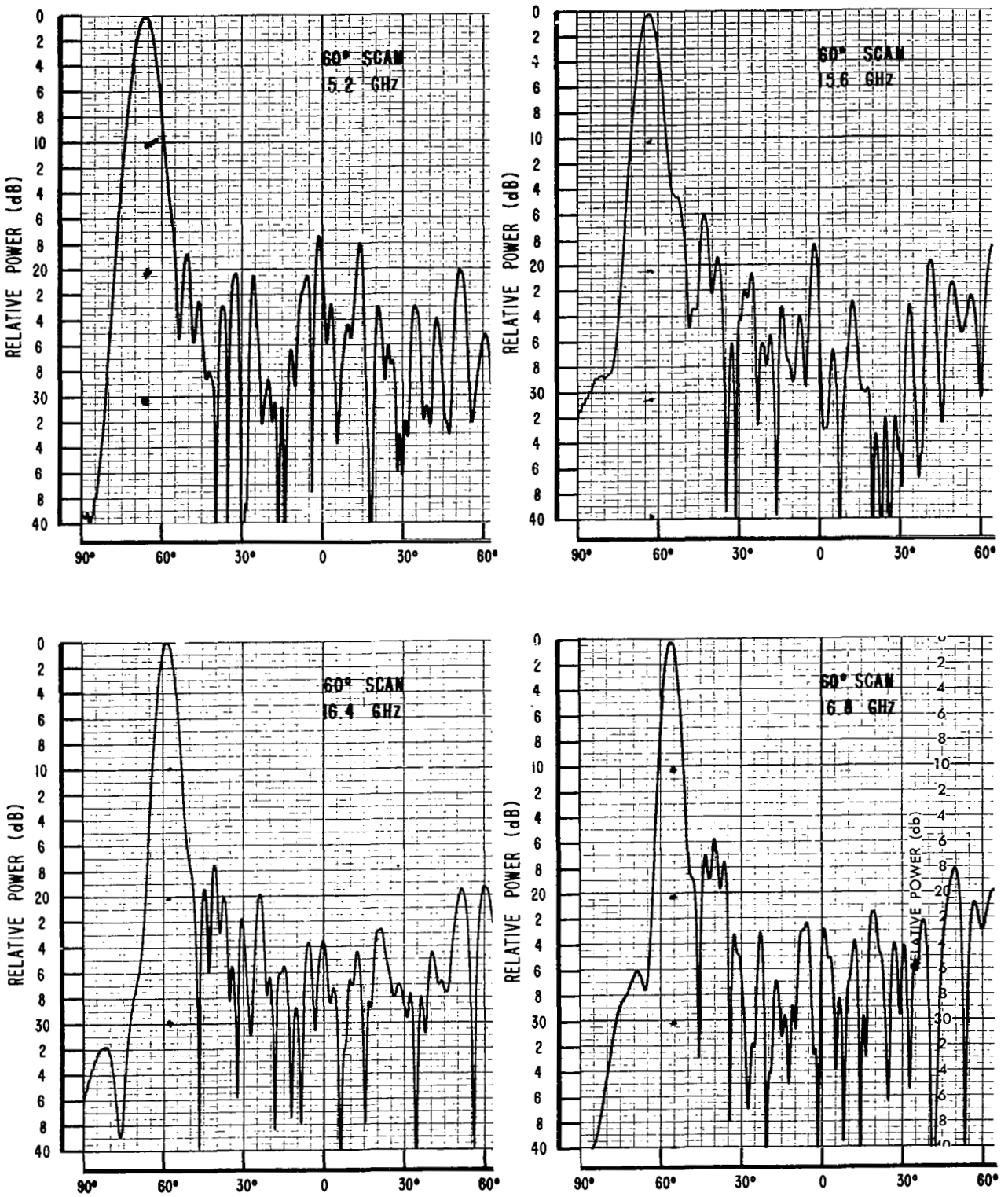

Figure 11(d). Array E-Plane Patterns - 60° Scan

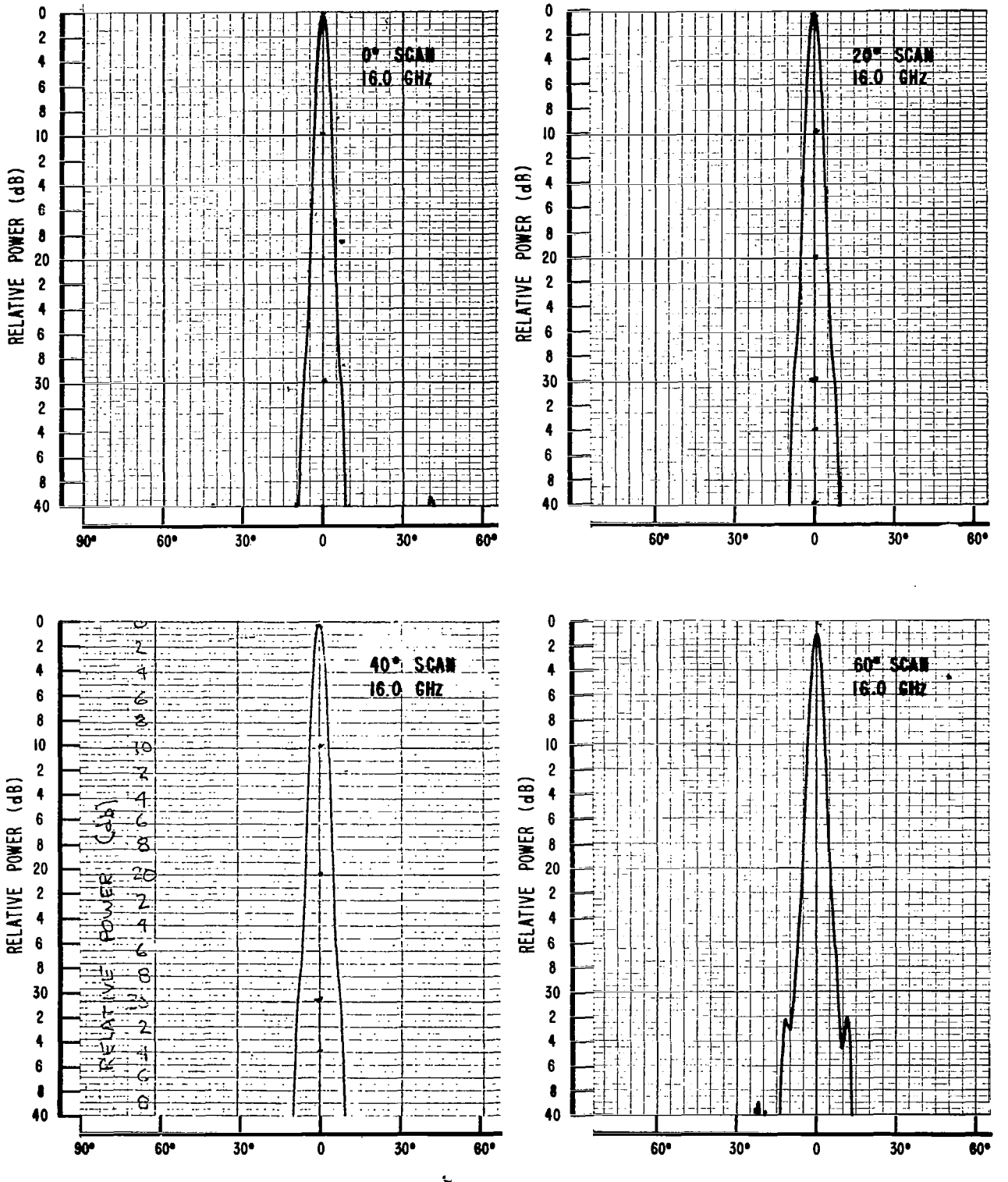

Figure 12. Array H-Plane Patterns - 16.0 GHz

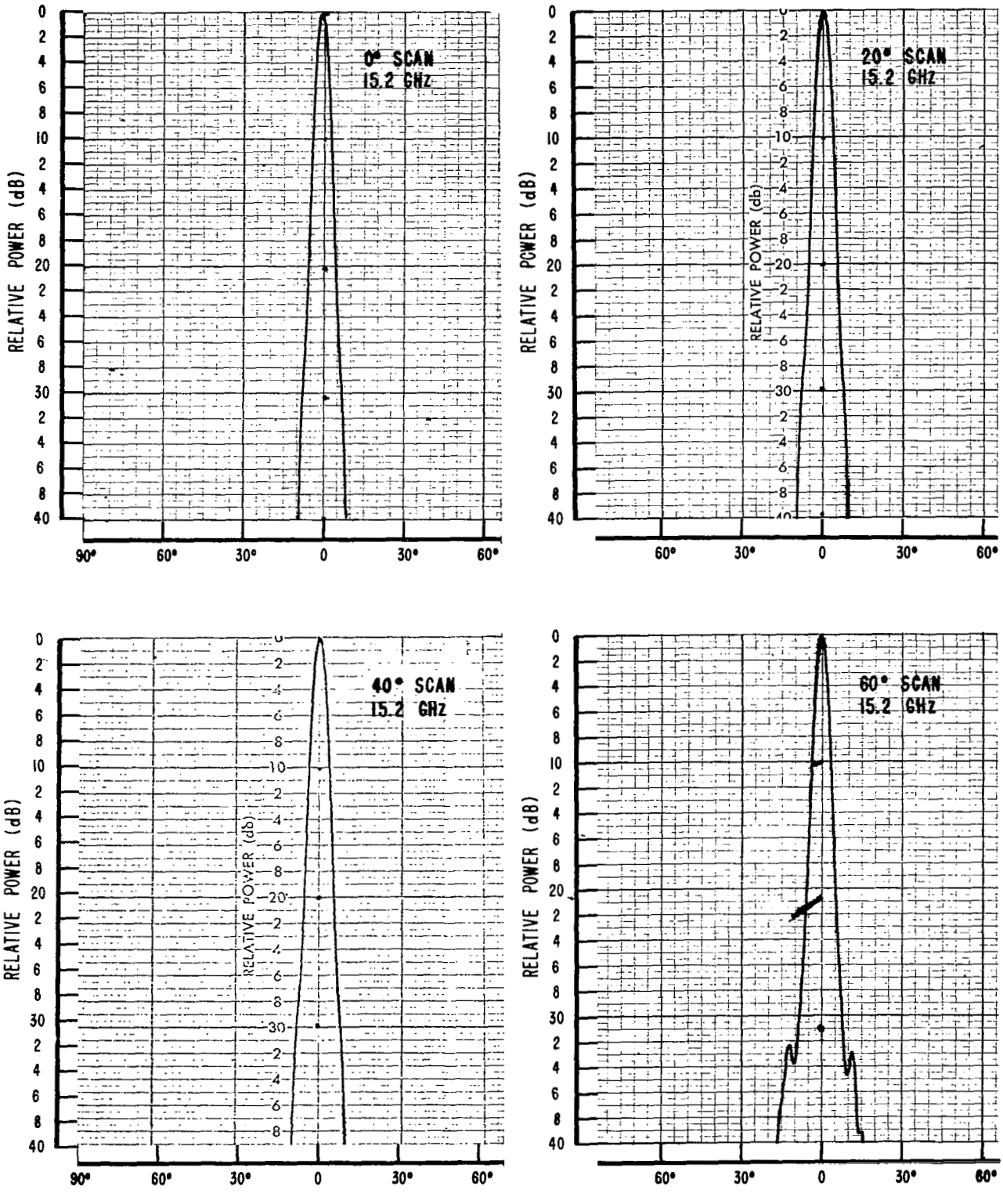

Figure 13(a). Array H-Plane Patterns - 15.2 GHz

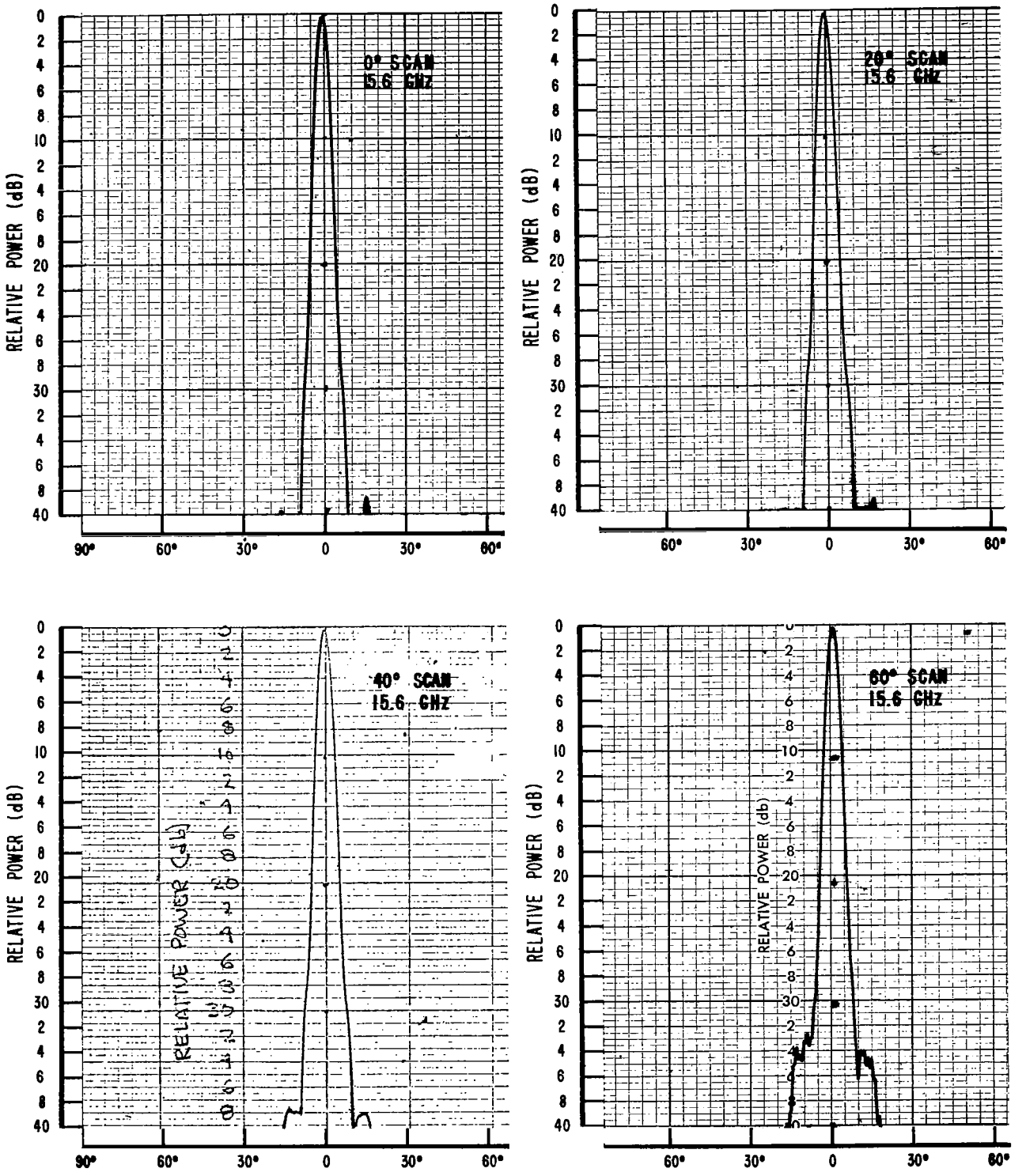

Figure 13(b). Array H-Plane Patterns - 15.6 GHz

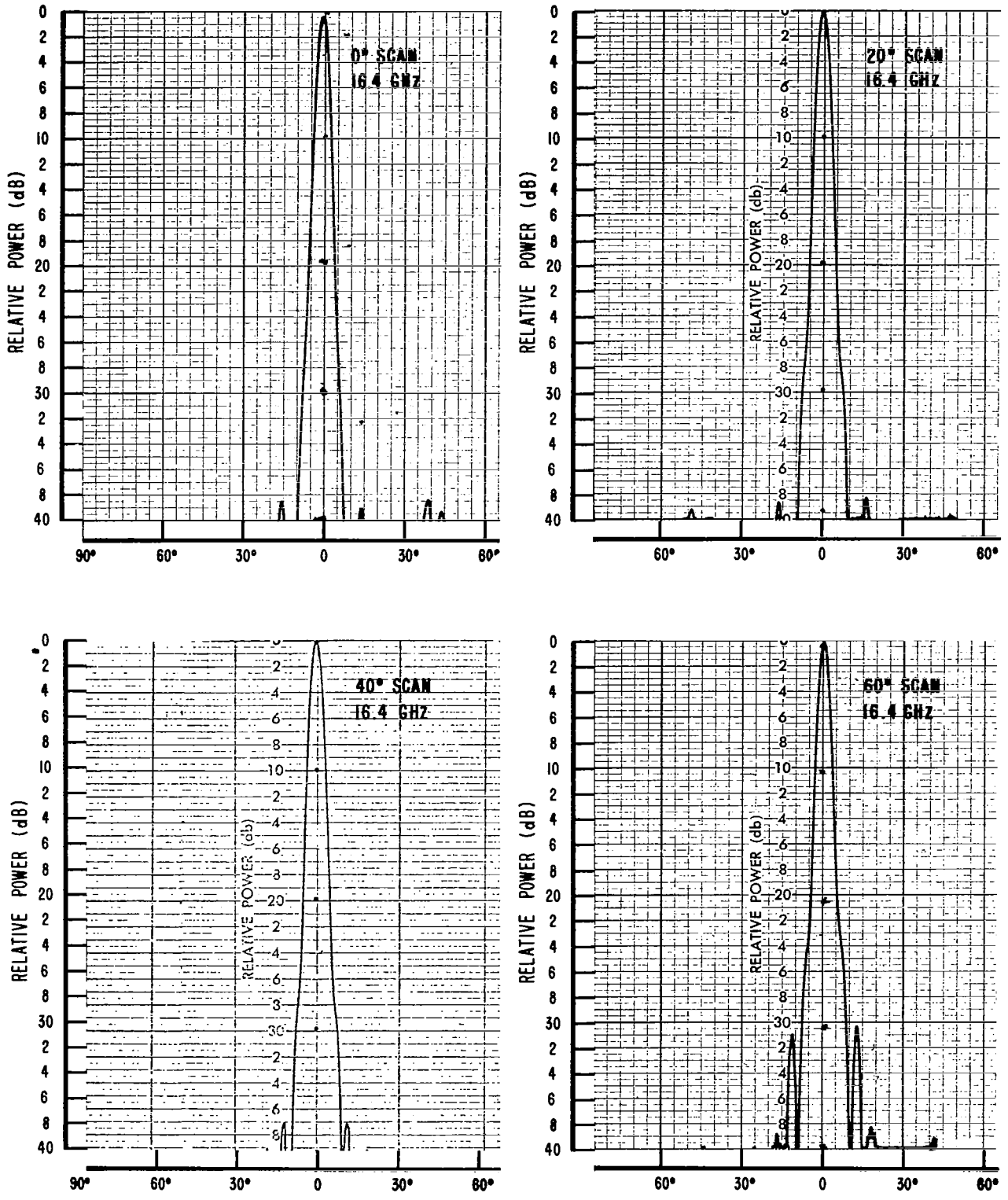

Figure 13(c). Array H-Plane Patterns - 16.4 GHz

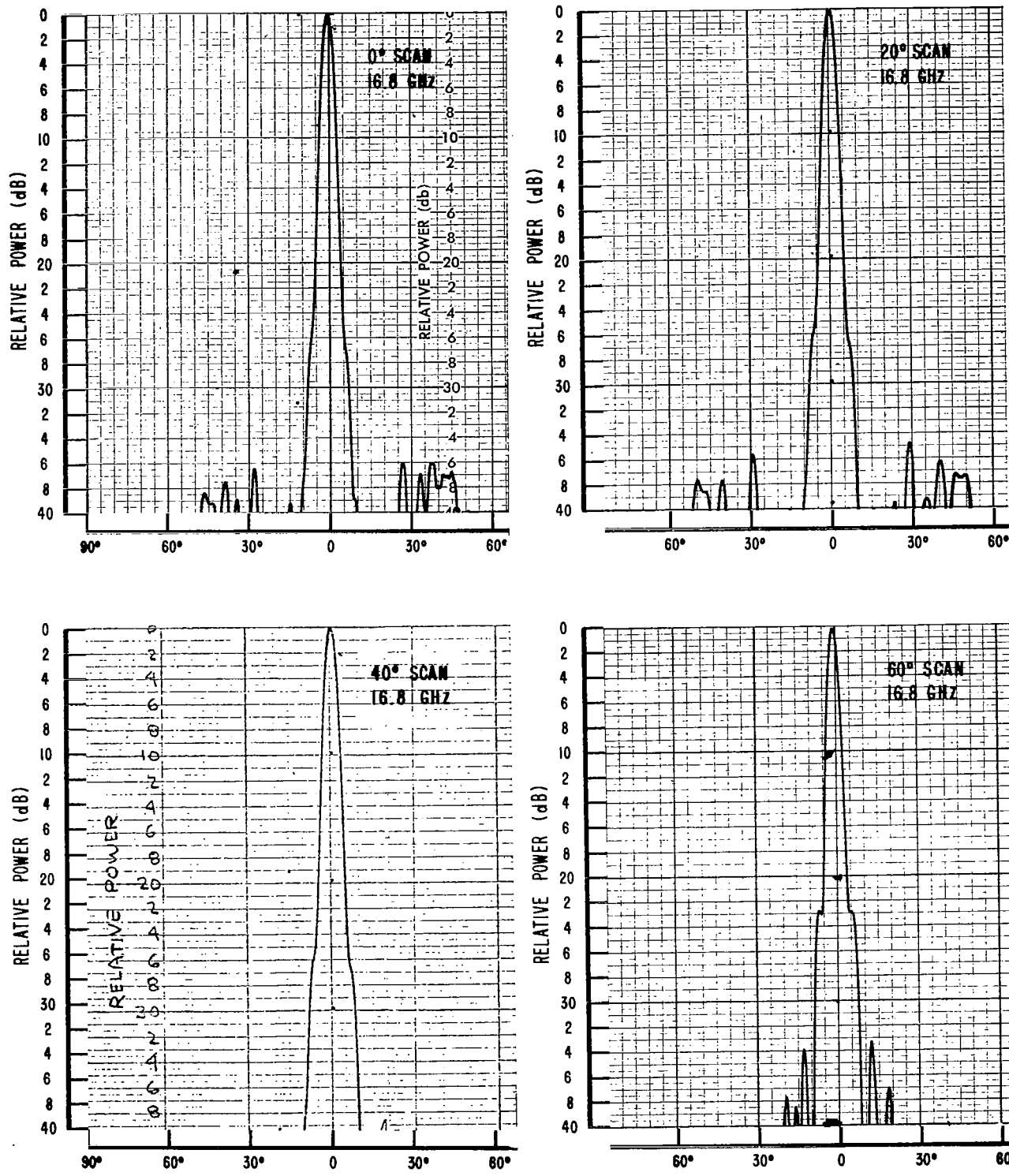

Figure 13(d). Array H-Plane Patterns - 16.8 GHz

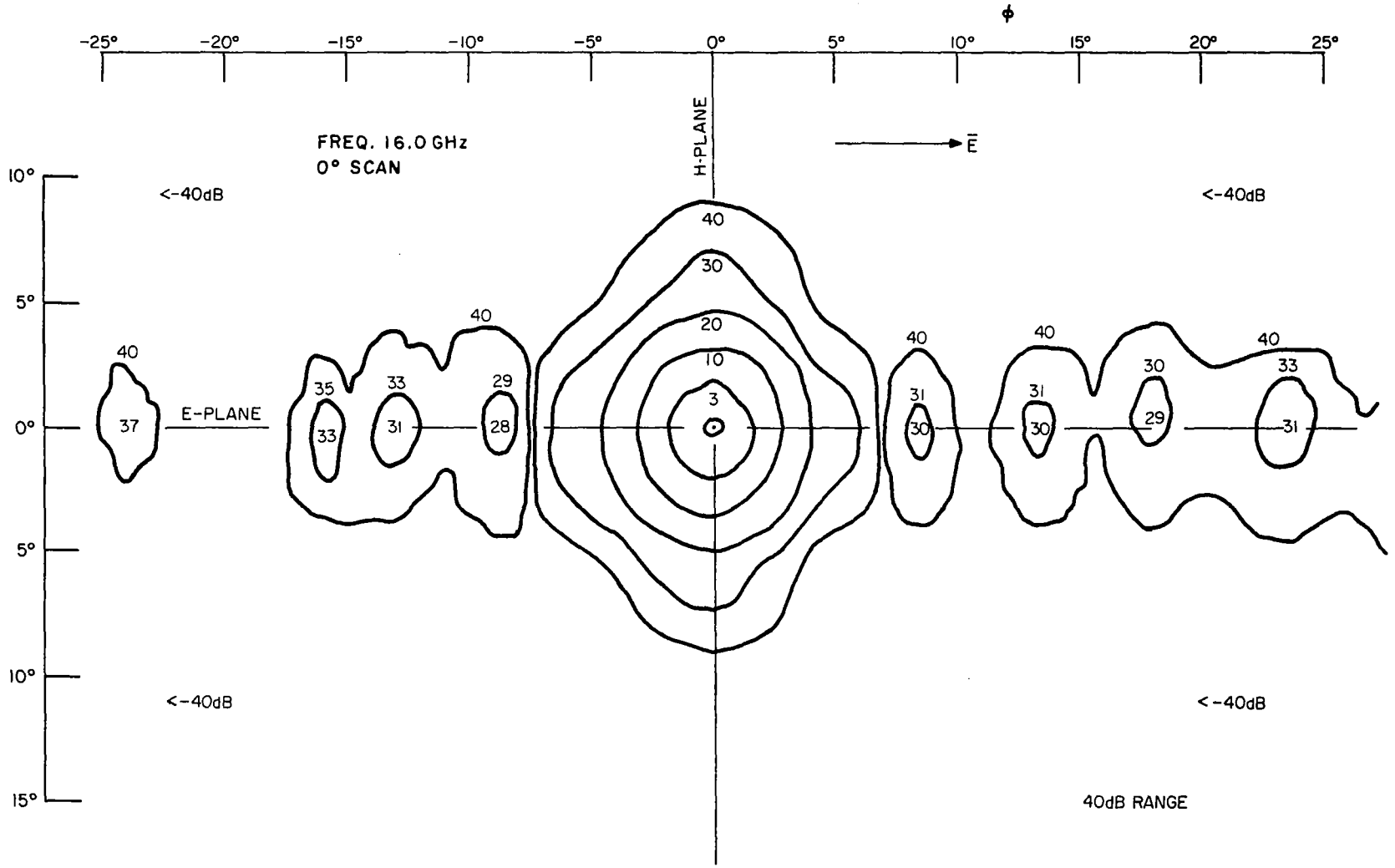

Figure 14(a). Low-Sidelobe Array, 0^{o} Scan (16.0 GHz)

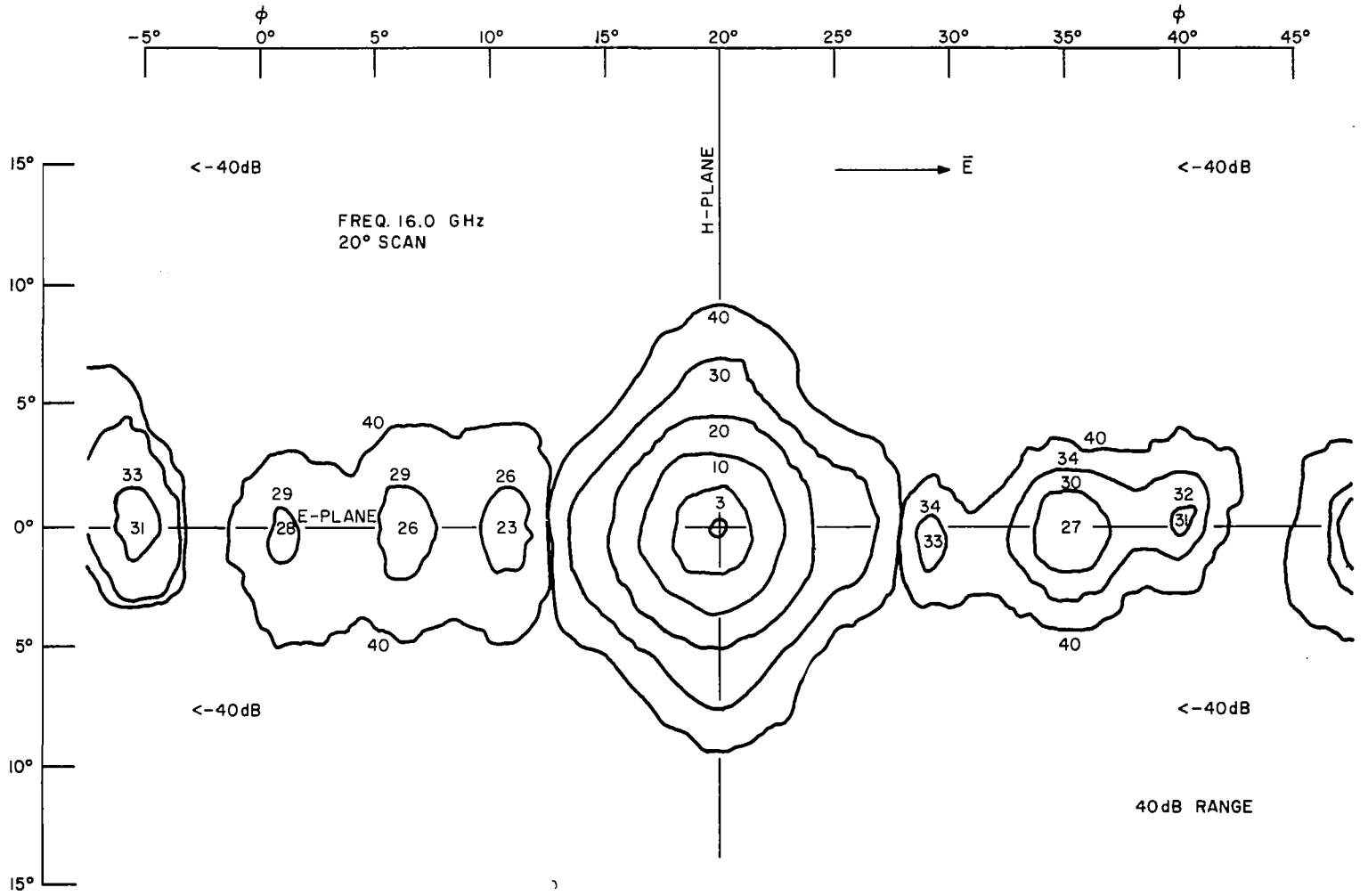

Figure 14(b). Low Sidelobe Array, 20° Scan (16.0 GHz)

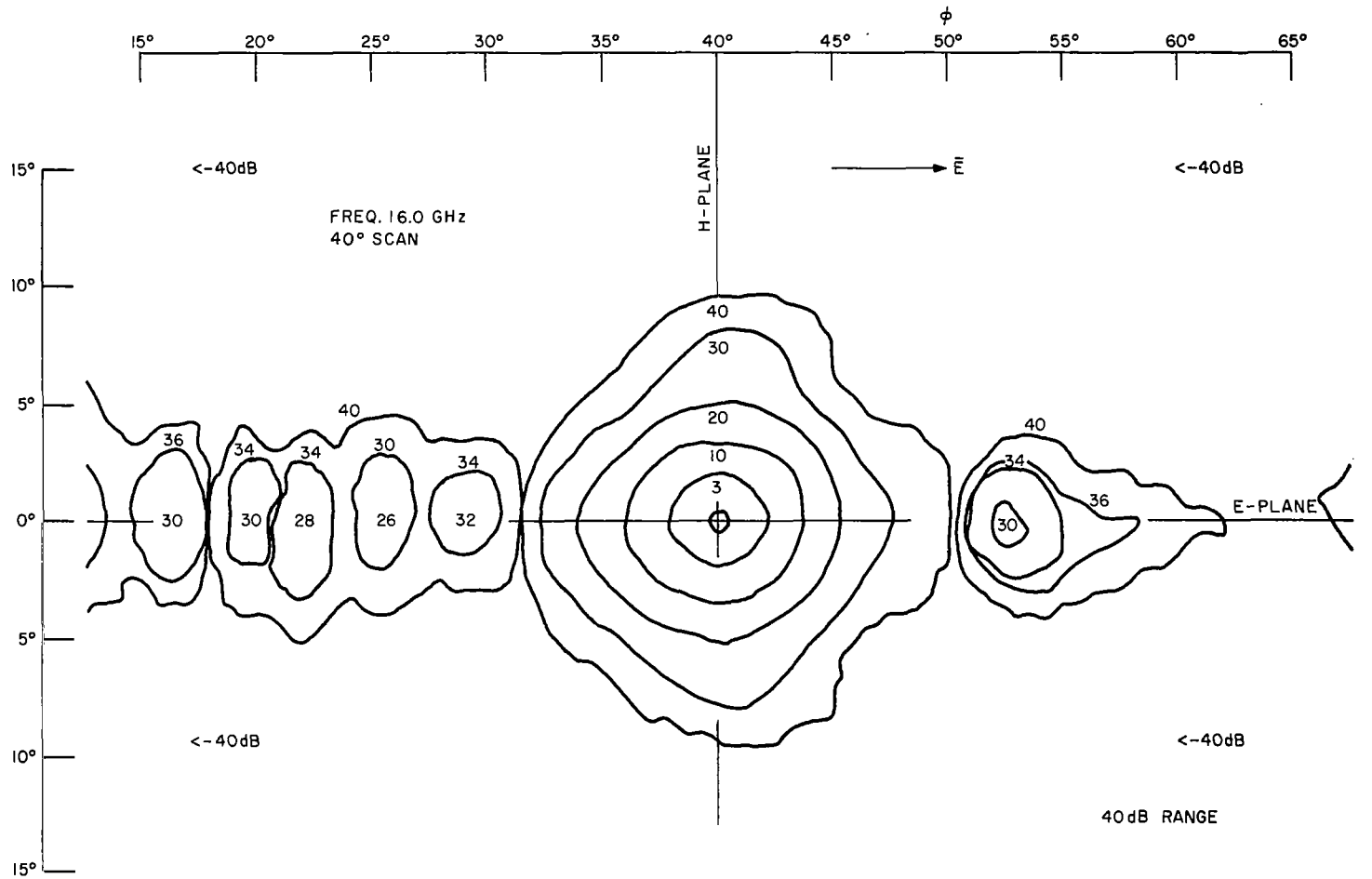

Figure 14(c). Low Sidelobe Array, 40^{o} Scan (16.0 GHz)

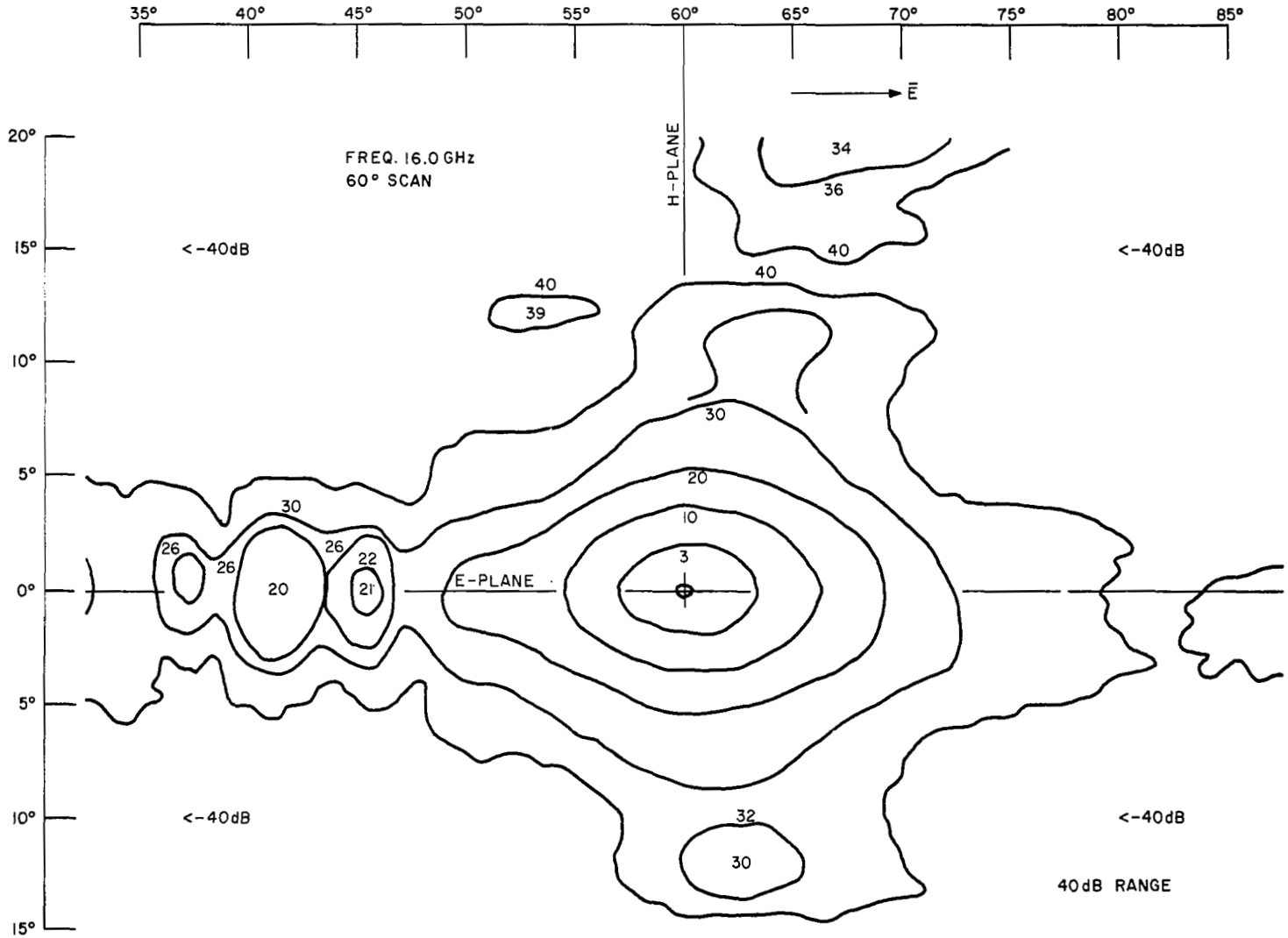

Figure 14(d). Low Sidelobe Array, 60° Scan (16.0 GHz)

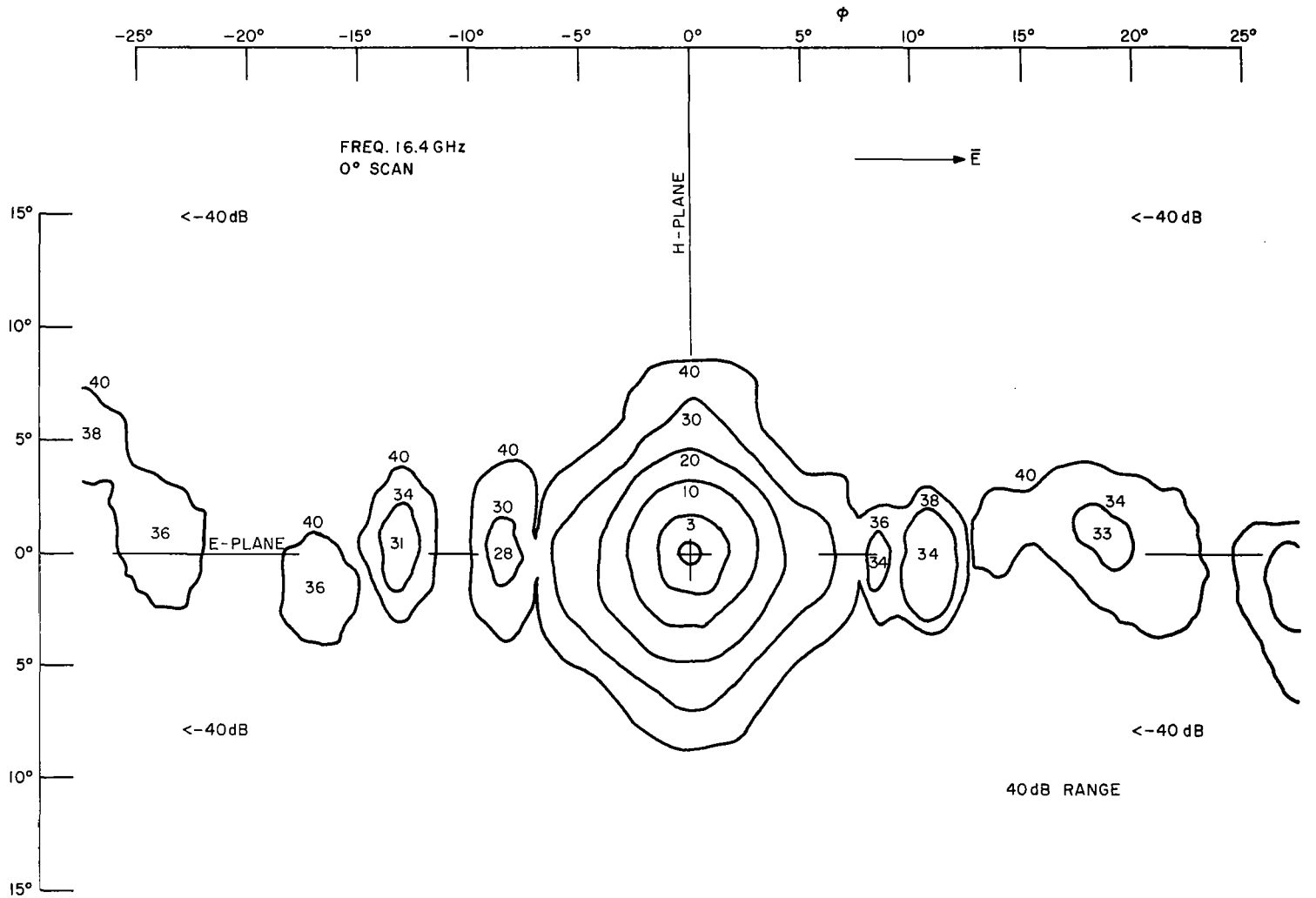

Figure 15(a). Low-Sidelobe Array, 0^{O} Scan (16.4 GHz)

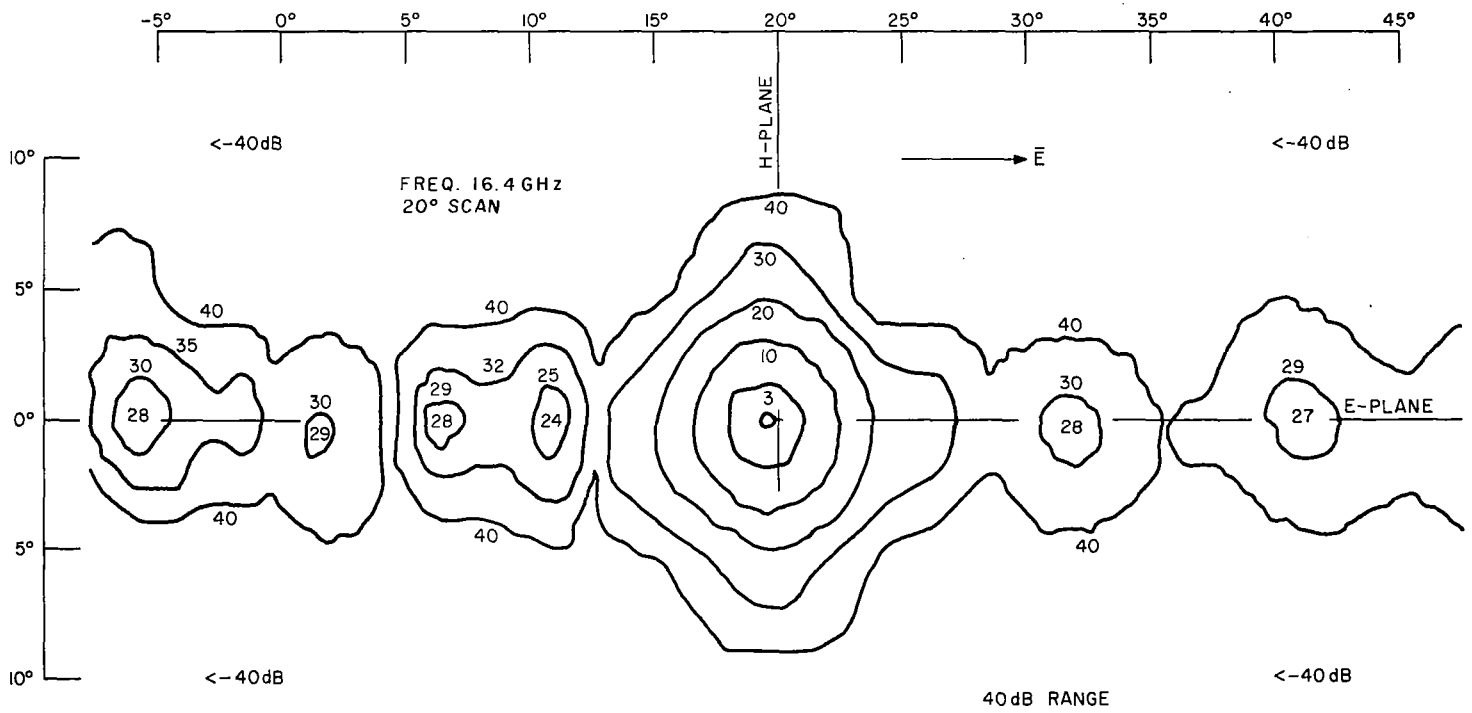

Figure 15(b). Low-Sidelobe Array, 20° Scan (16.4 GHz)

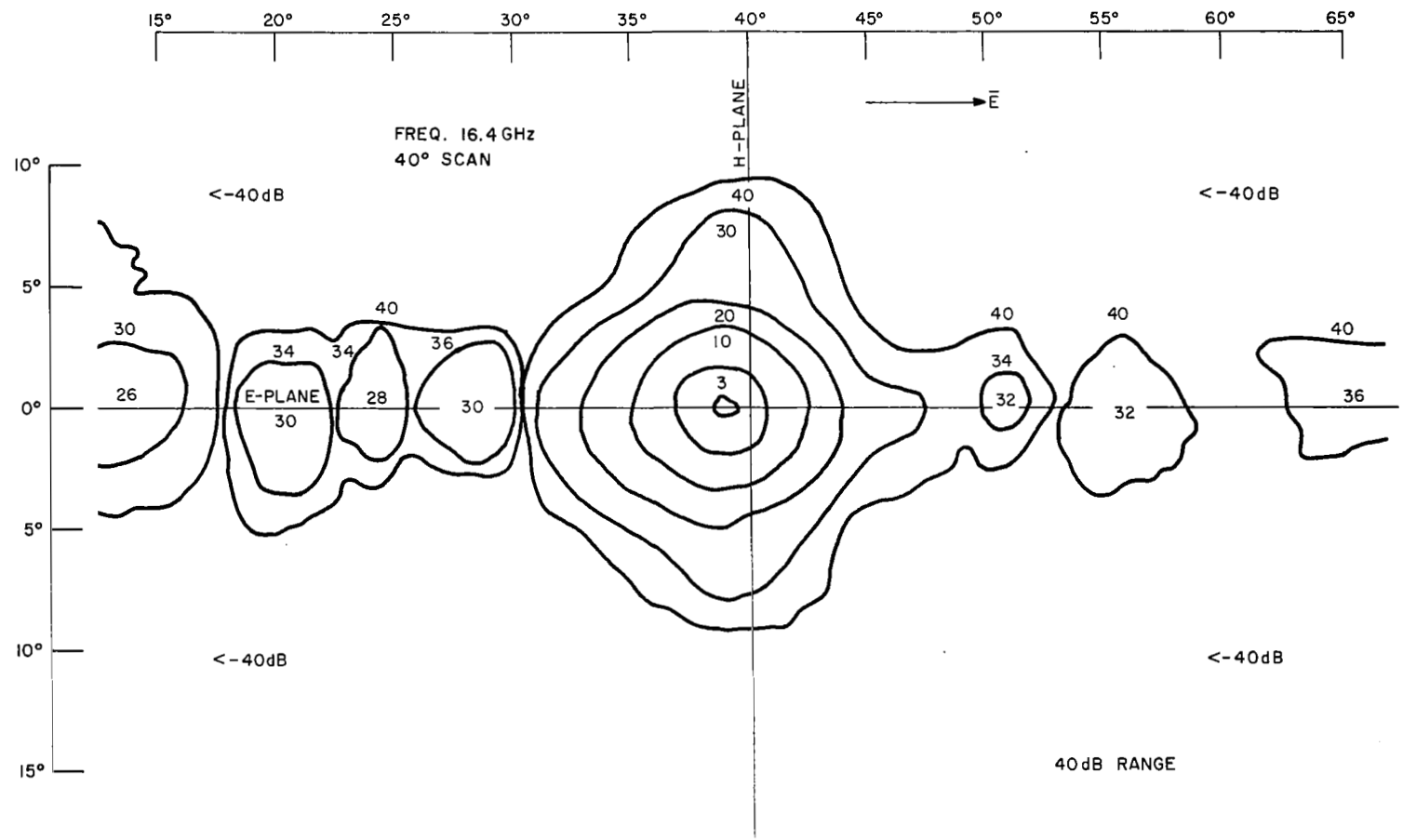

Figure 15(c). Low Sidelobe Array, 40^{o} Scan (16.4 GHz)

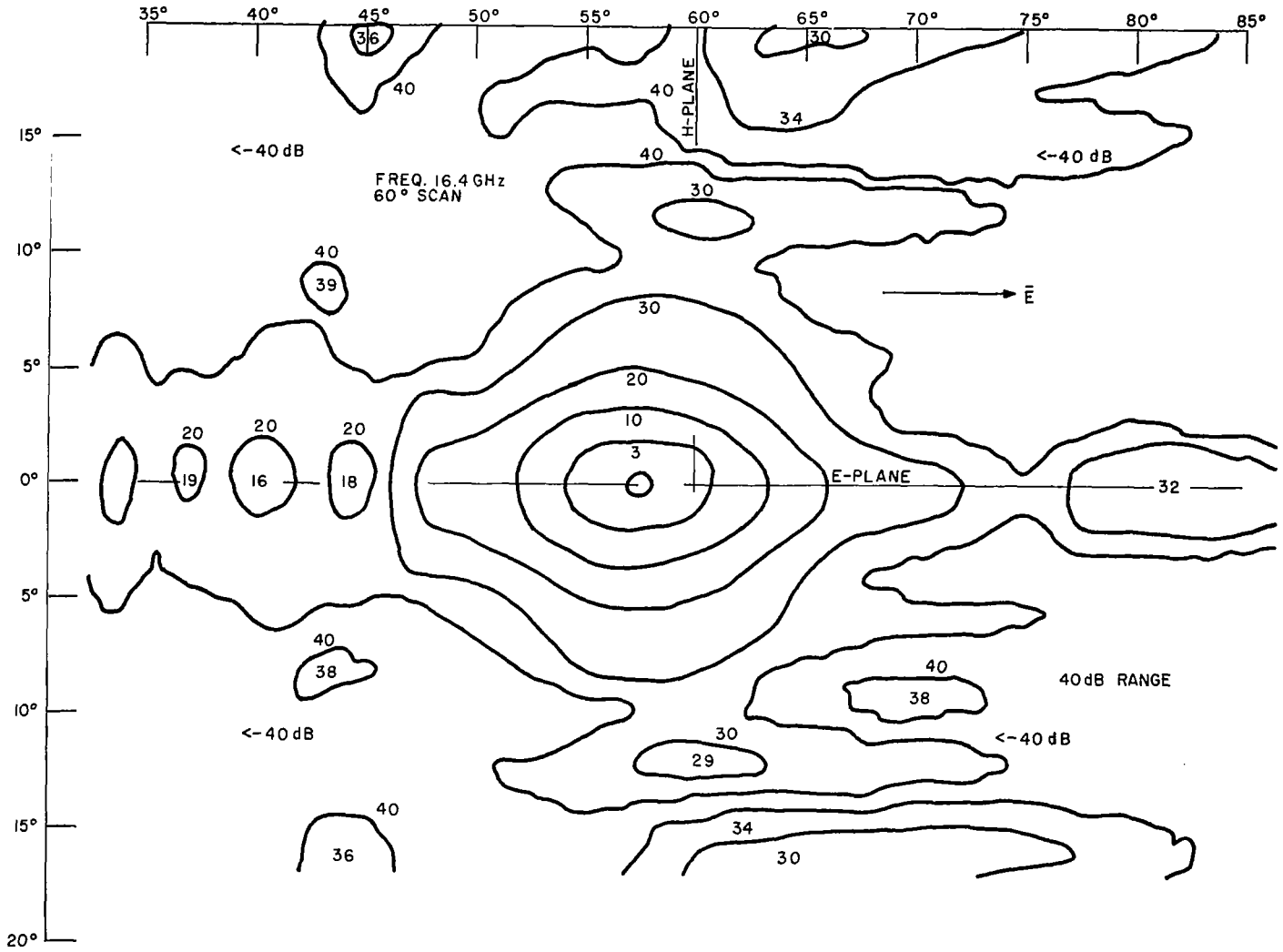

Figure 15(d). Low Sidelobe Array, 60^{O} Scan (16.4 GHz)

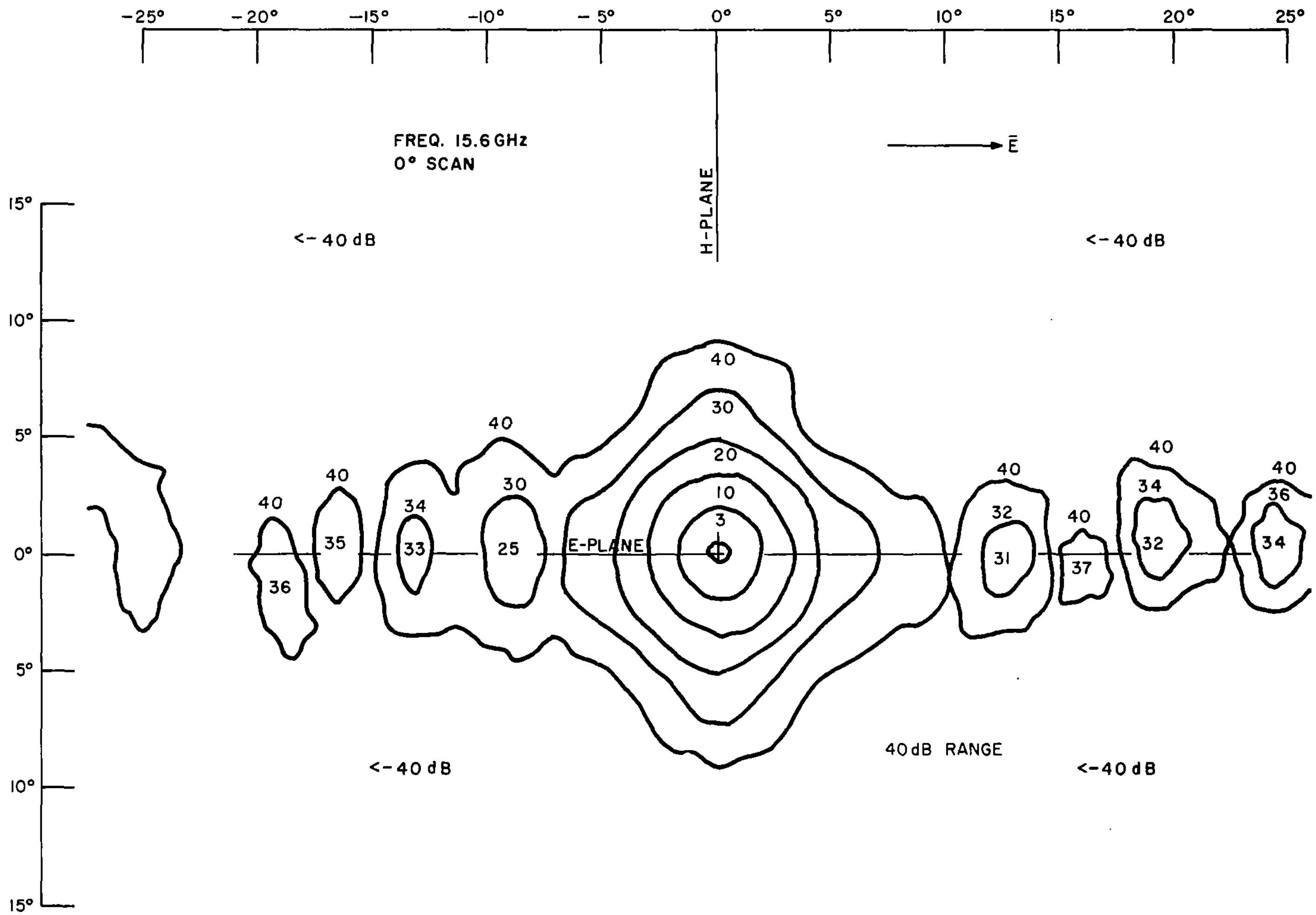

Figure 15(e). Low Sidelobe Array, 0° Scan (15.6 GHz)

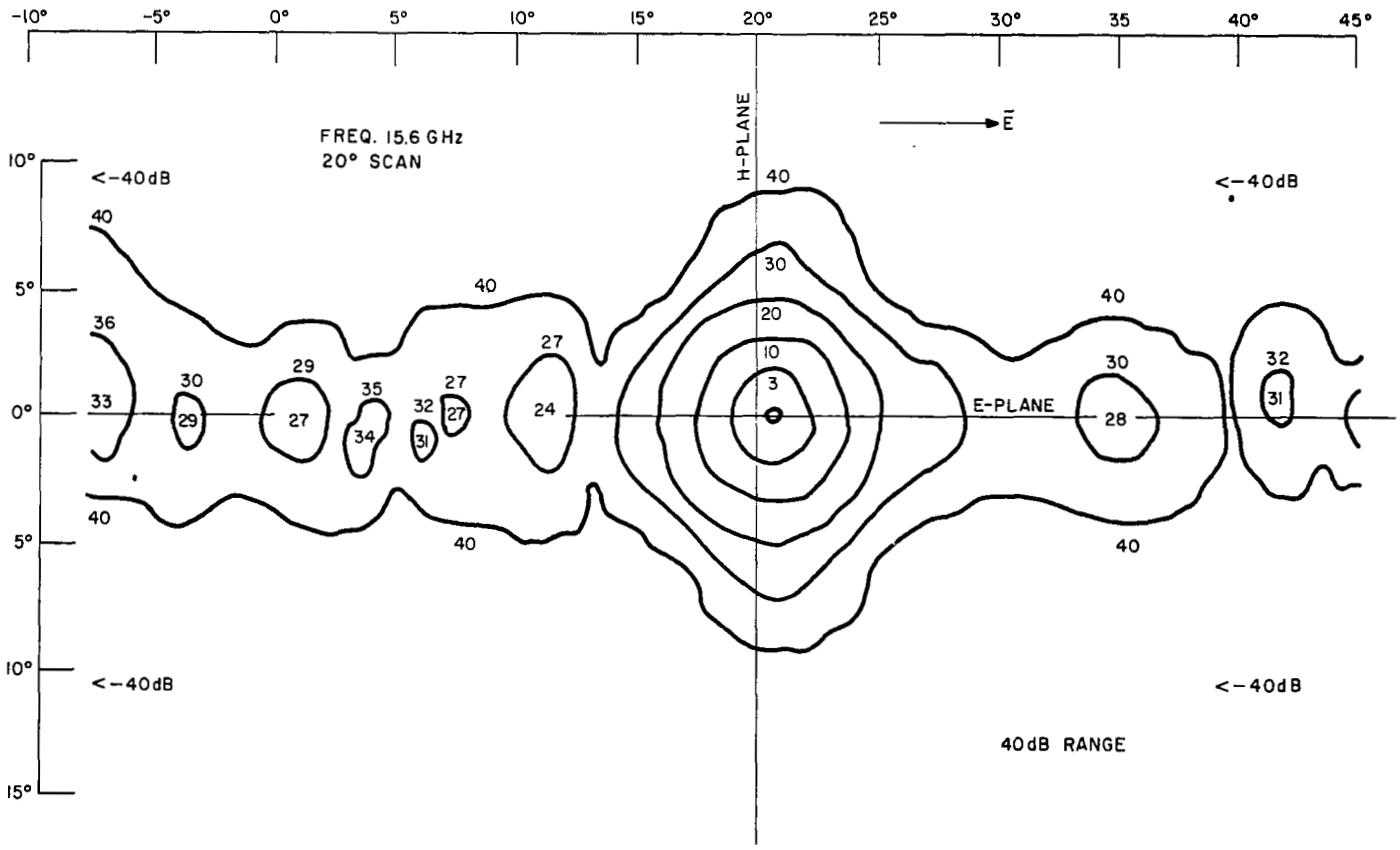

Figure 15(f). Low Sidelobe Array, 20^{0} Scan (15.6 GHz)

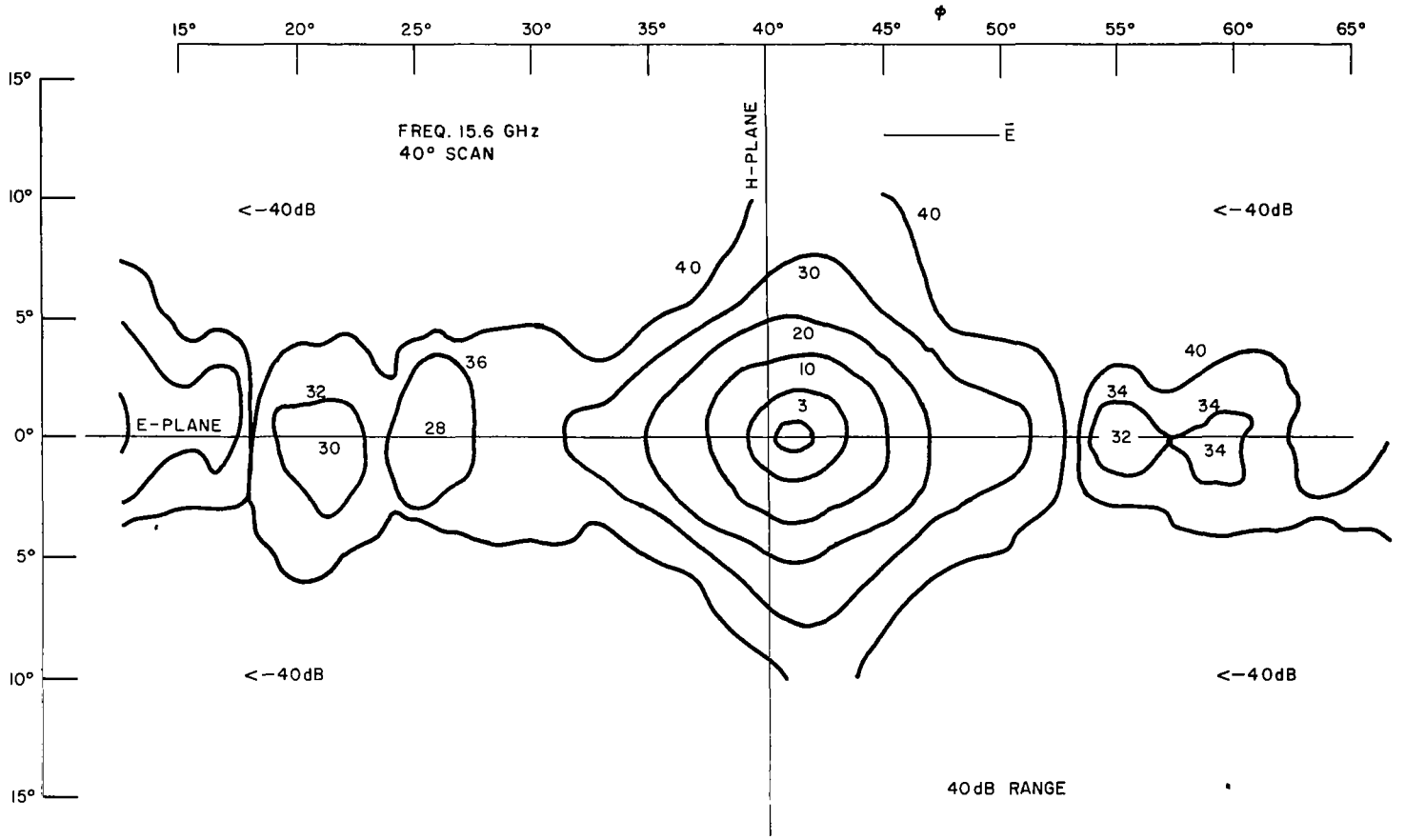

Figure 15(g). Low Sidelobe Array, 40^{o} Scan (15.6 GHz)

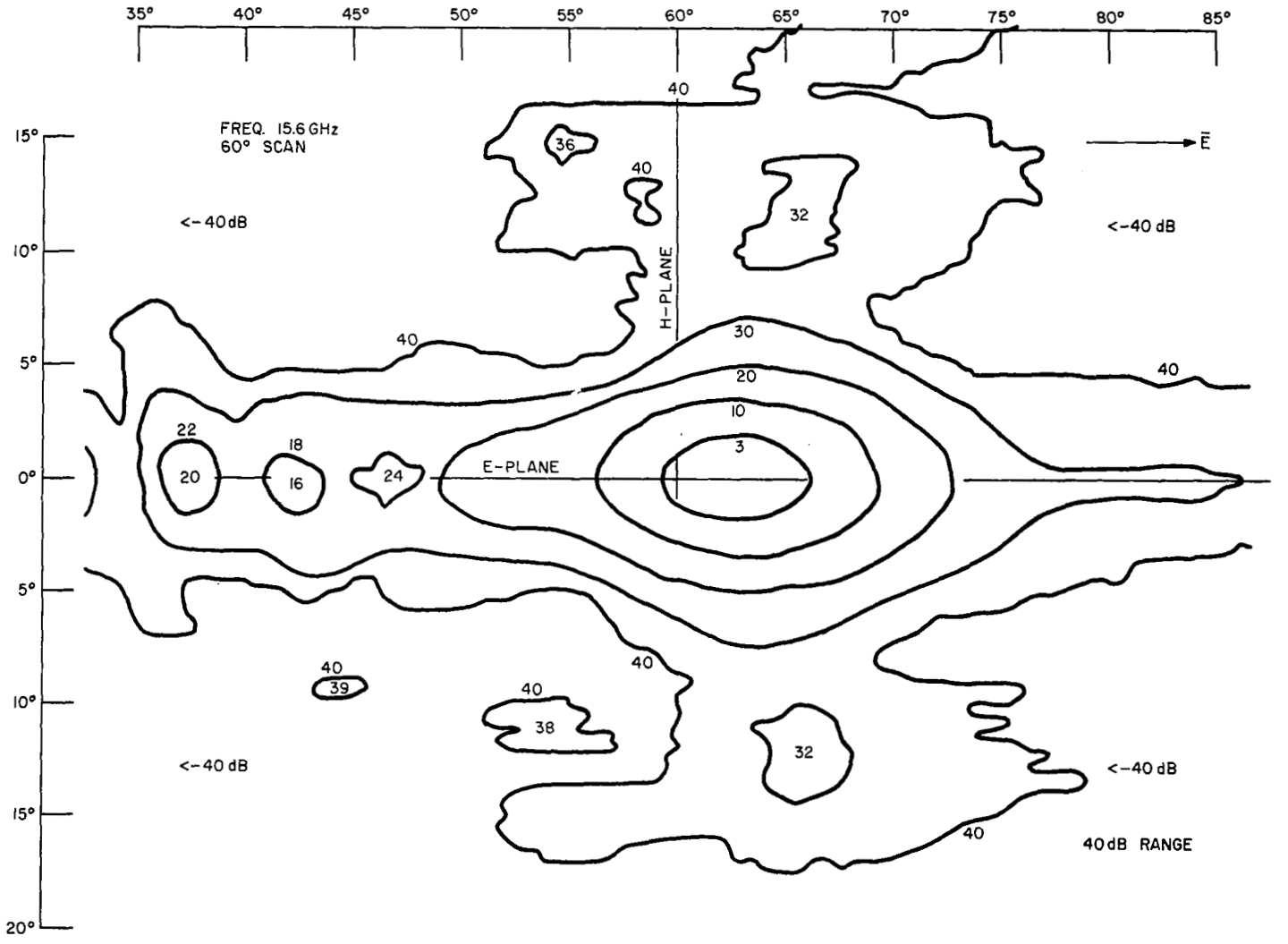

Figure 15(h). Low Sidelobe Array, 60° Scan (15.6 GHz)

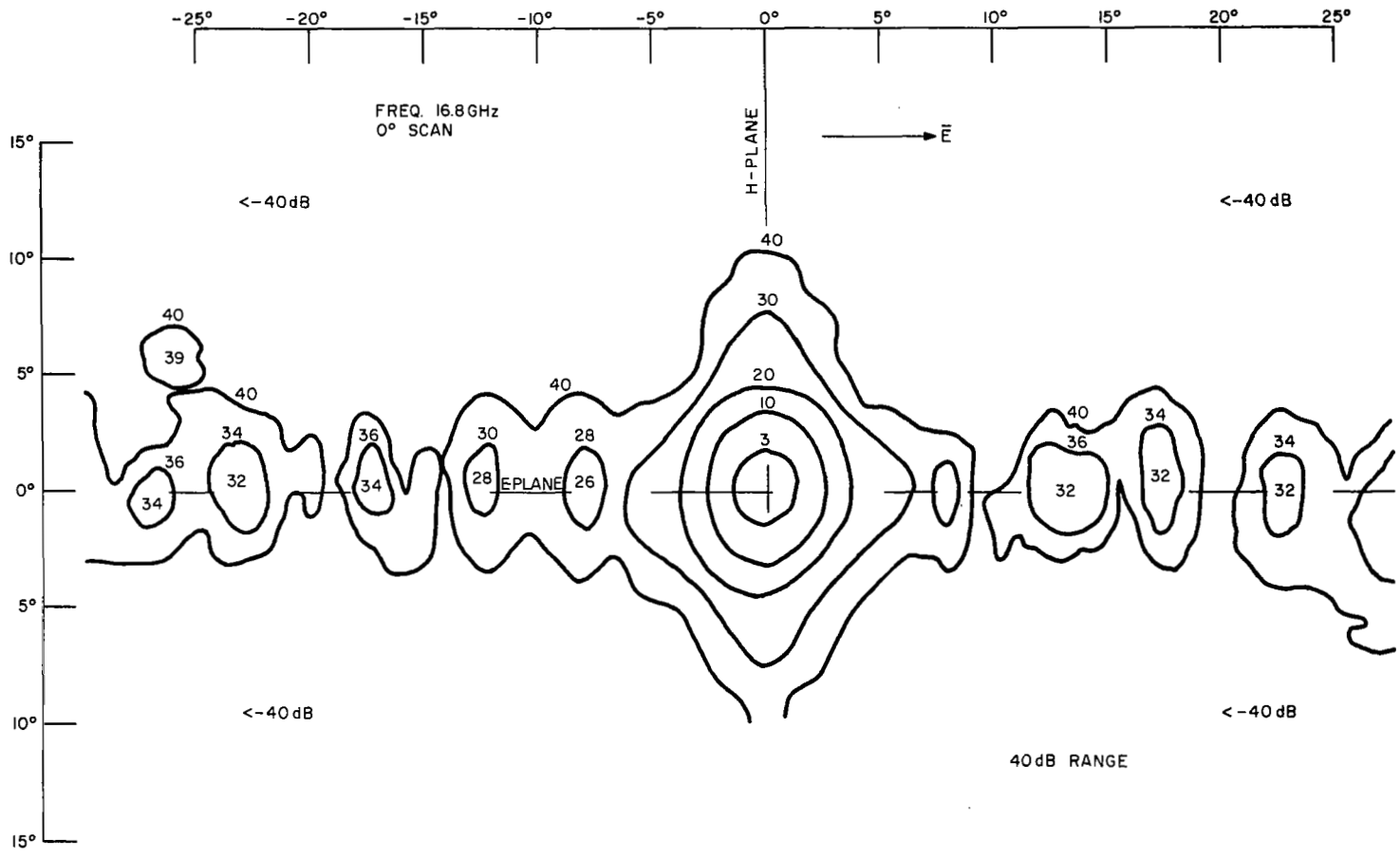

Figure 15(i). Low Sidelobe Array, 0^{o} Scan (16.8 GHz)

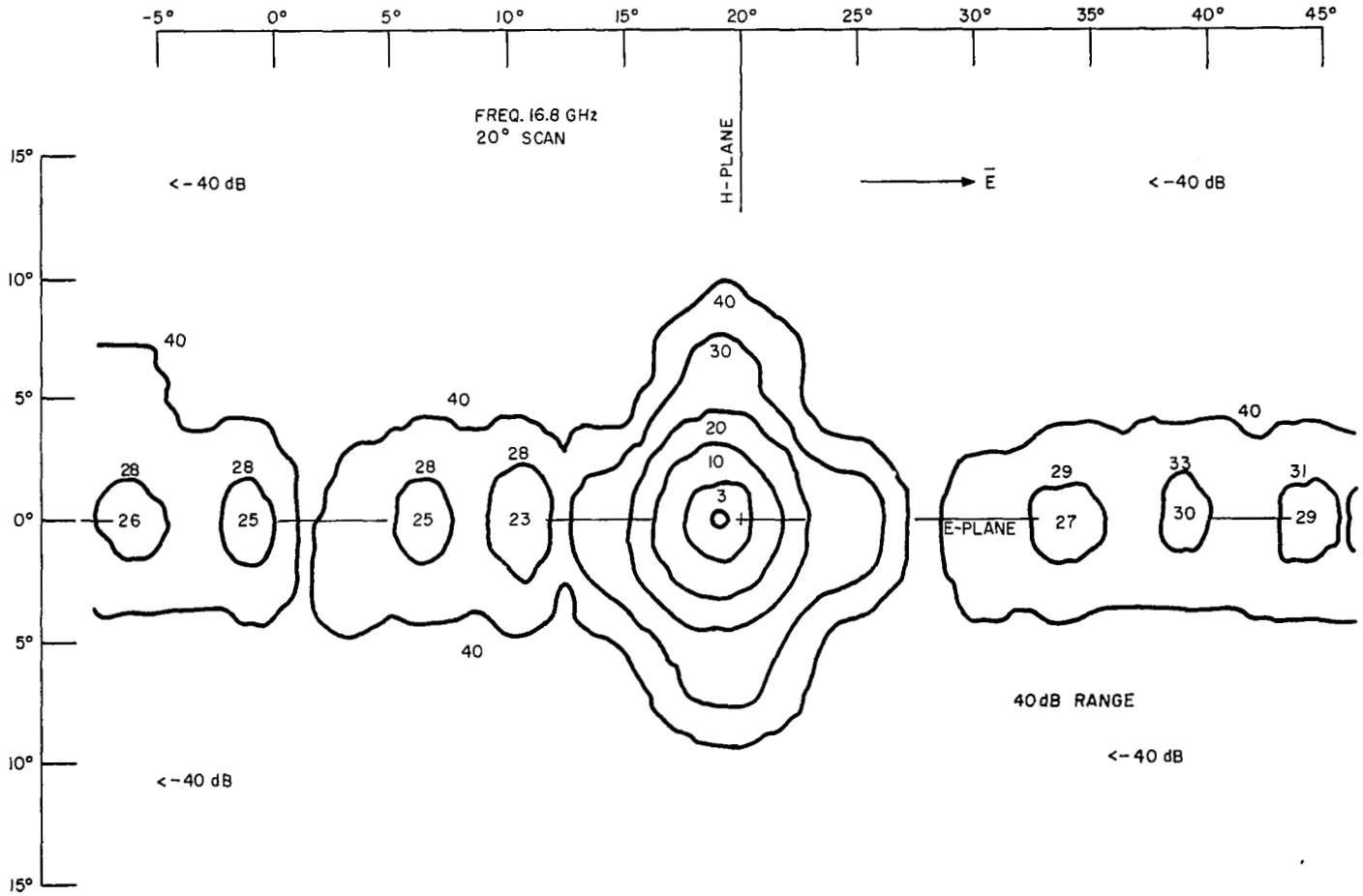

Figure 15(j). Low Sidelobe Array, 20° Scan (16.8 GHz)

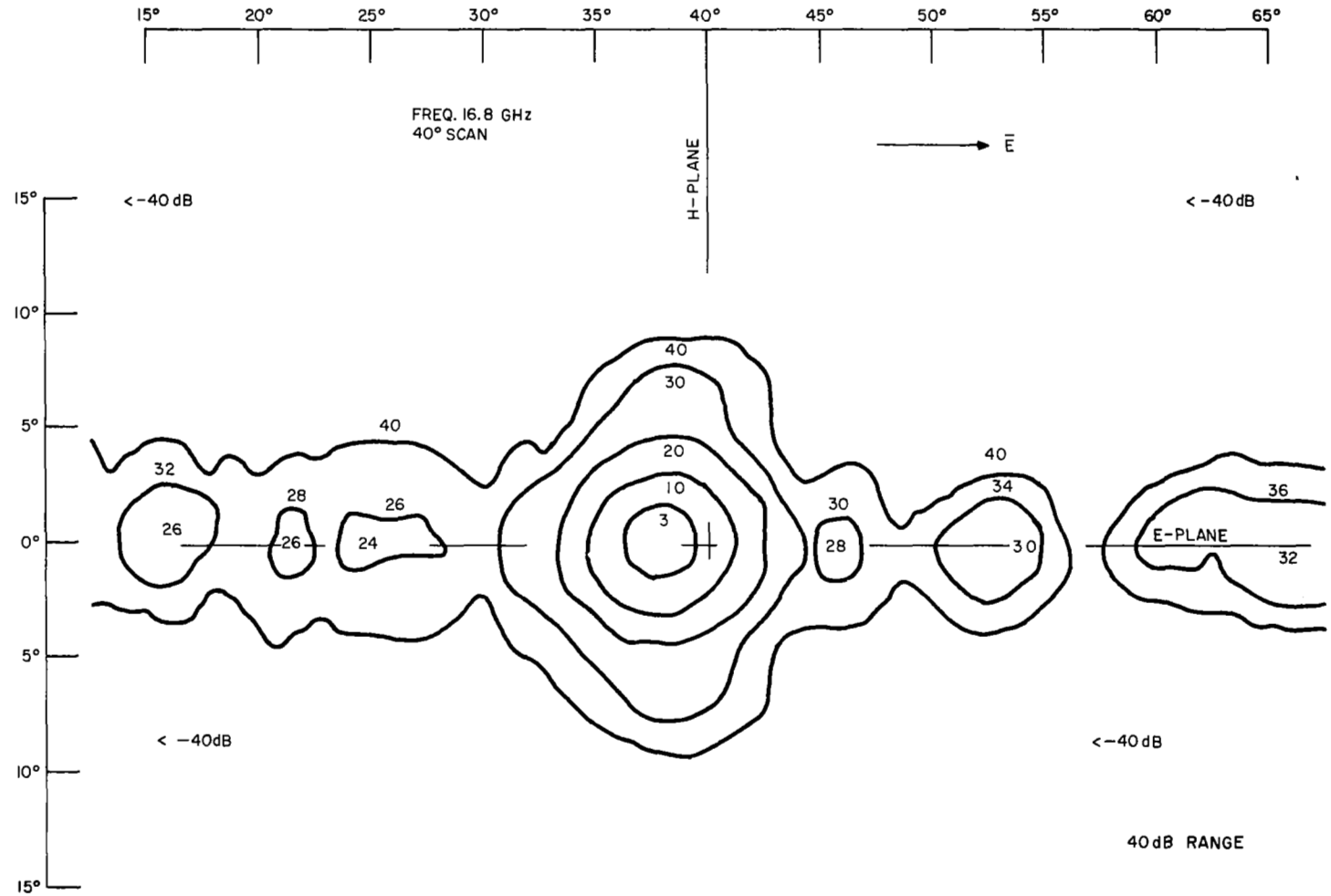

Figure 15(k). Low Sidelobe Array, 40^{o} Scan (16.8 GHz)

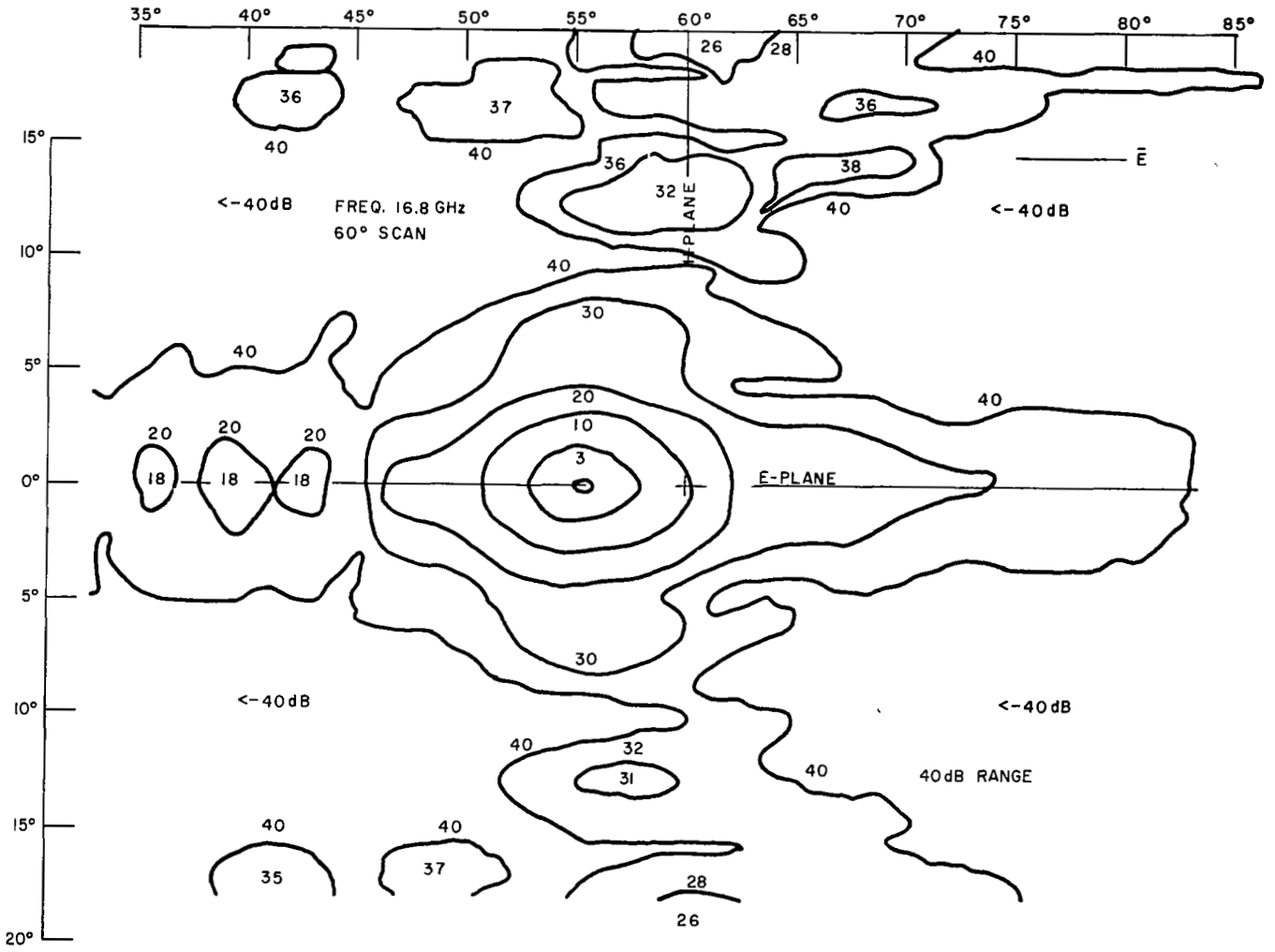

Figure 15(I). Low Sidelobe Array, 60° Scan (16.8 GHz)

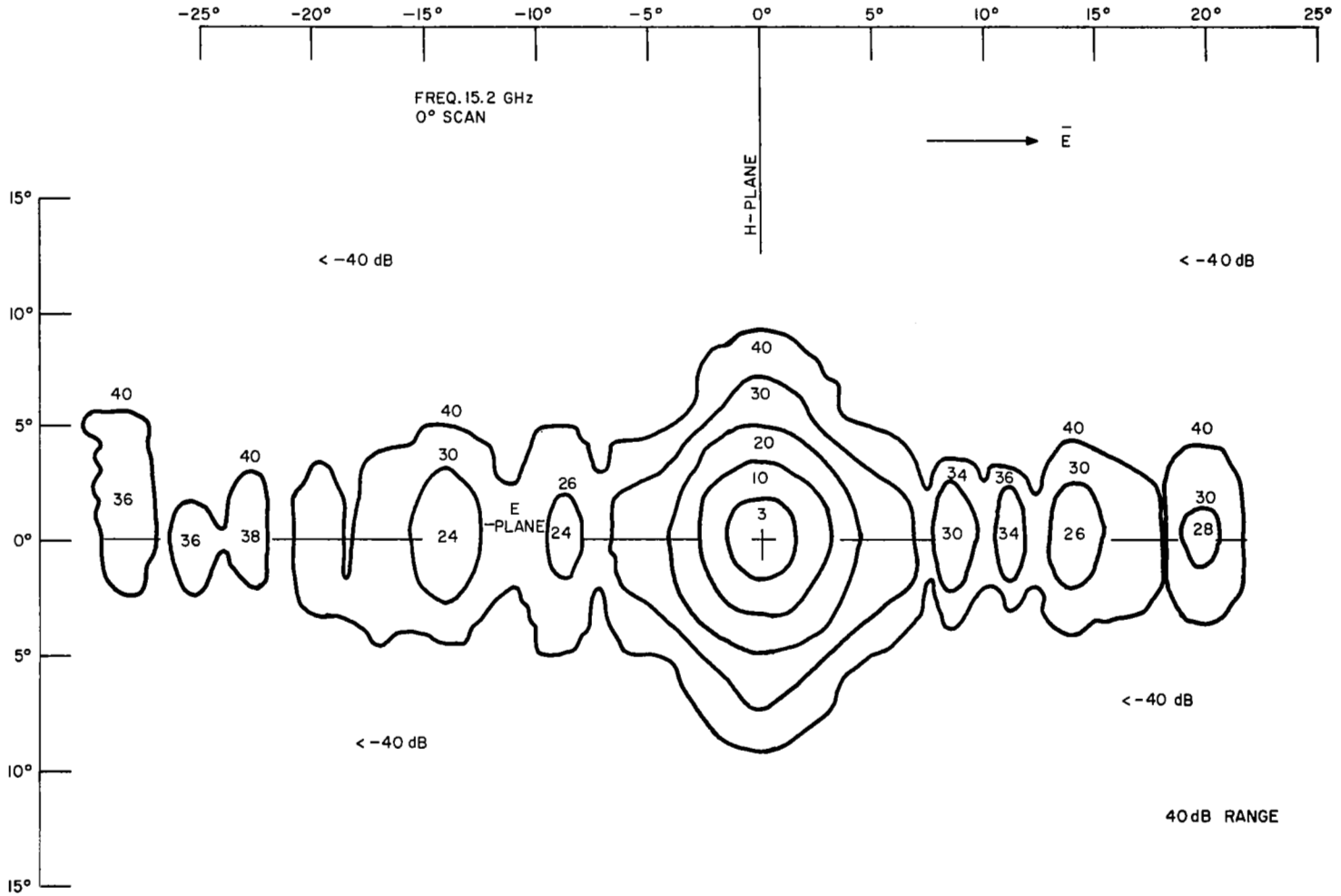

Figure 15(m). Low Sidelobe Array, 0^{o} Scan (15.2 GHz)

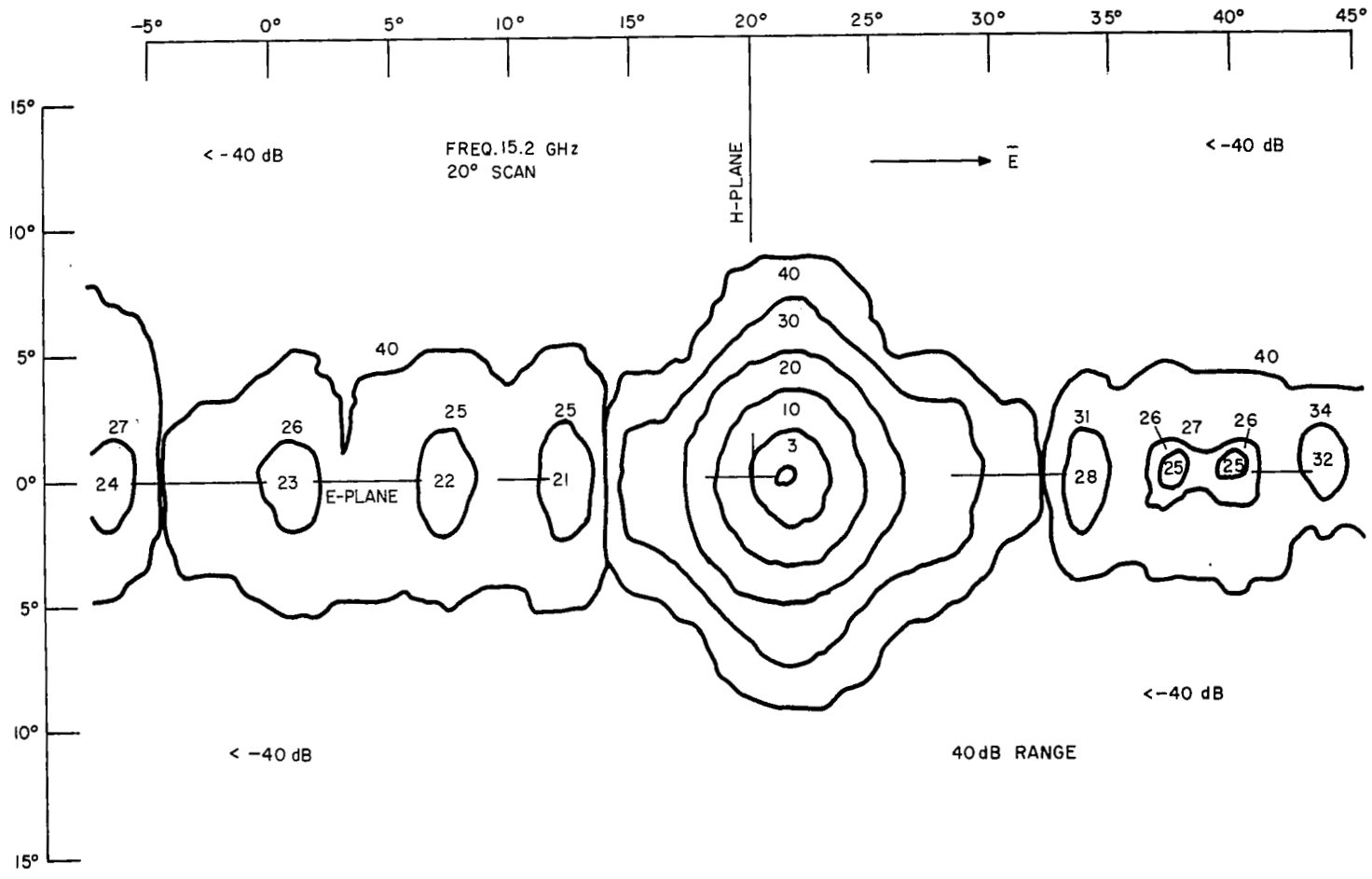

Figure 15(n). Low Sidelobe Array, 20^{o} Scan (15.2 GHz)

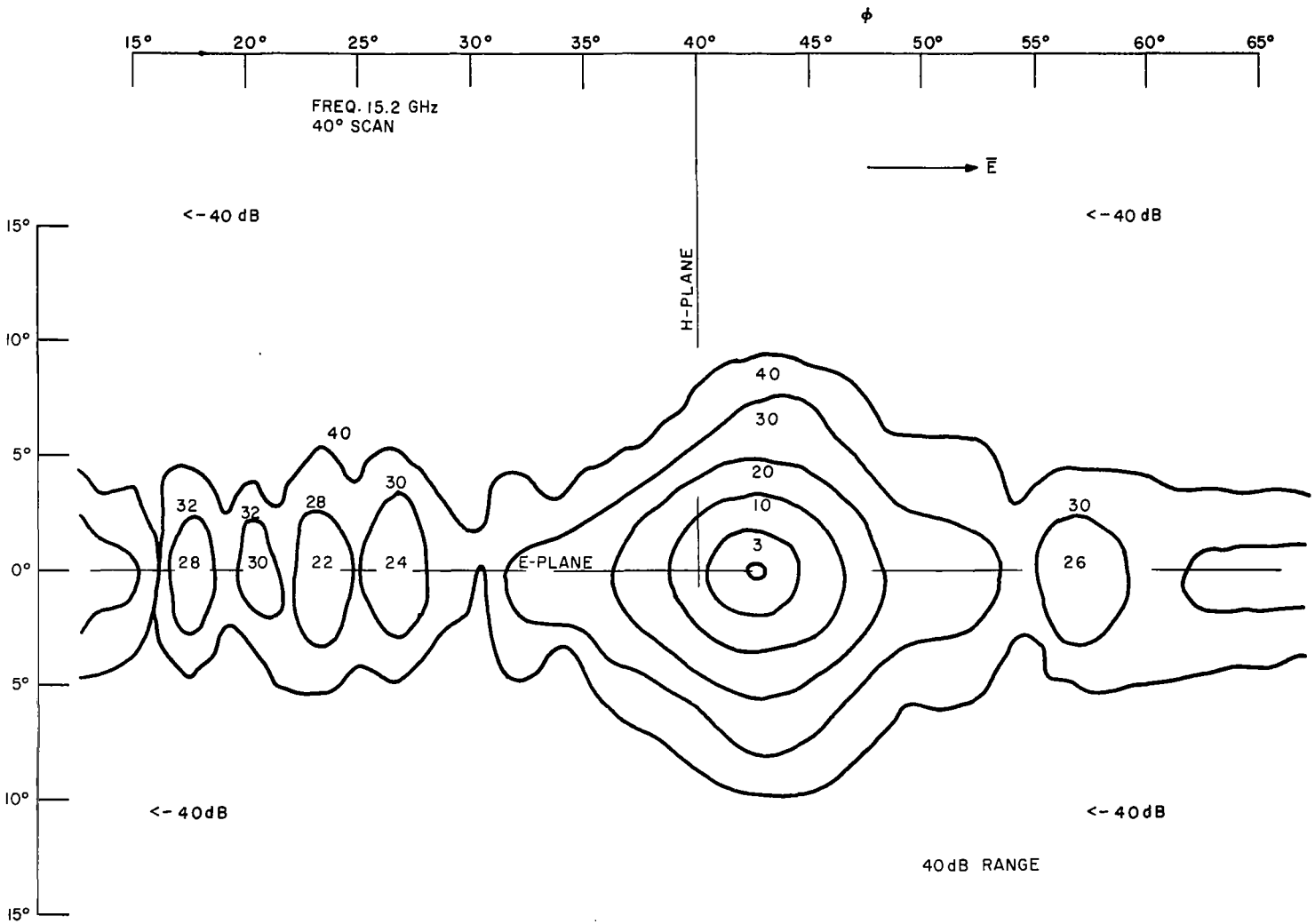

Figure 15(o). Low Sidelobe Array, 40° Scan (15.2 GHz)

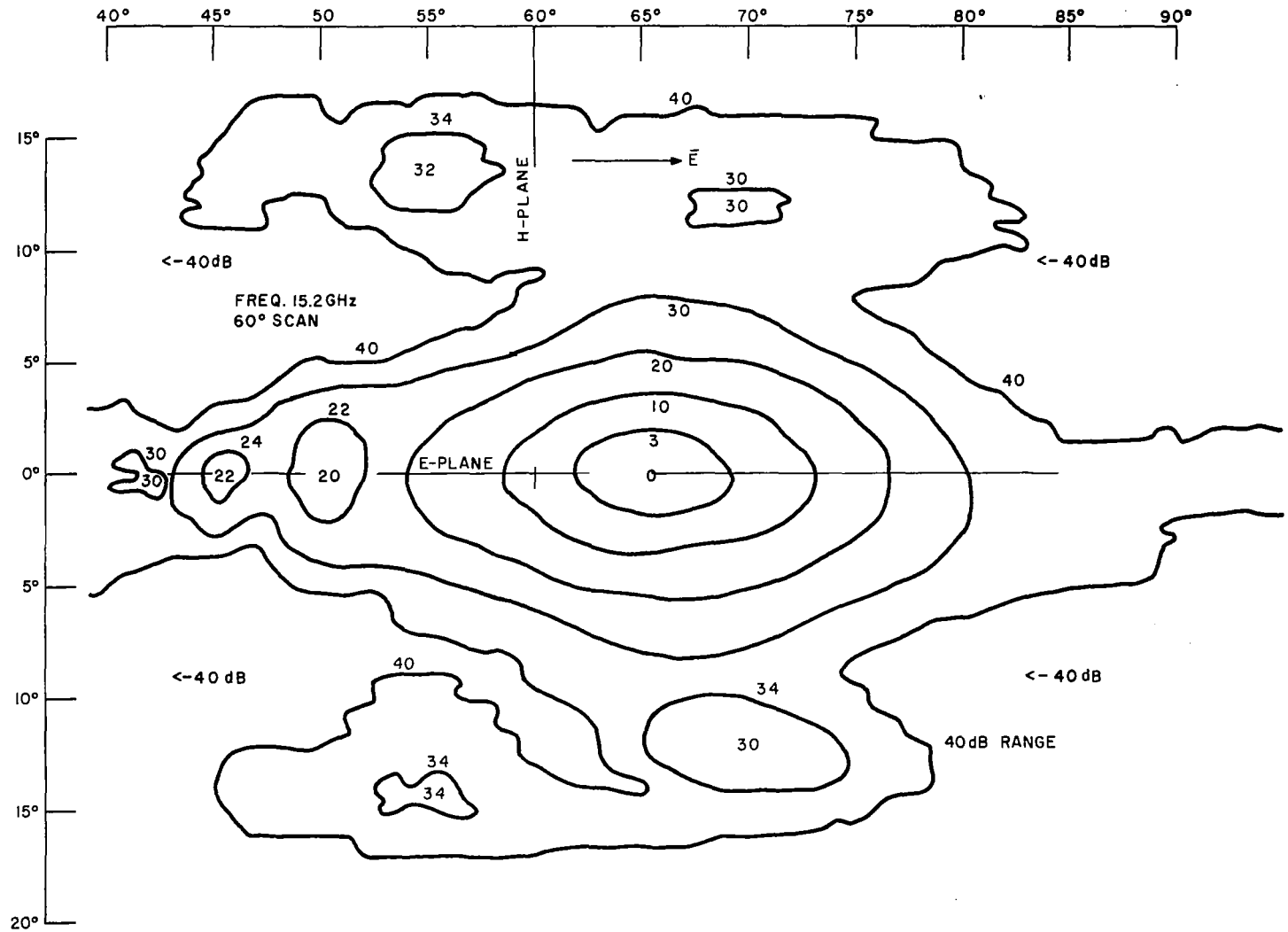

Figure 15(p). Low Sidelobe Array, 60^{o} Scan (15.2 GHz)

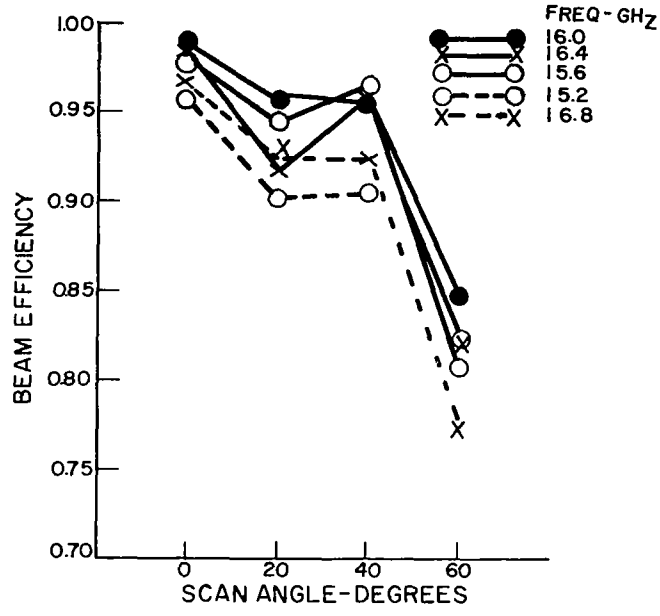

Figure 16. Beam Efficiency vs Scan Angle

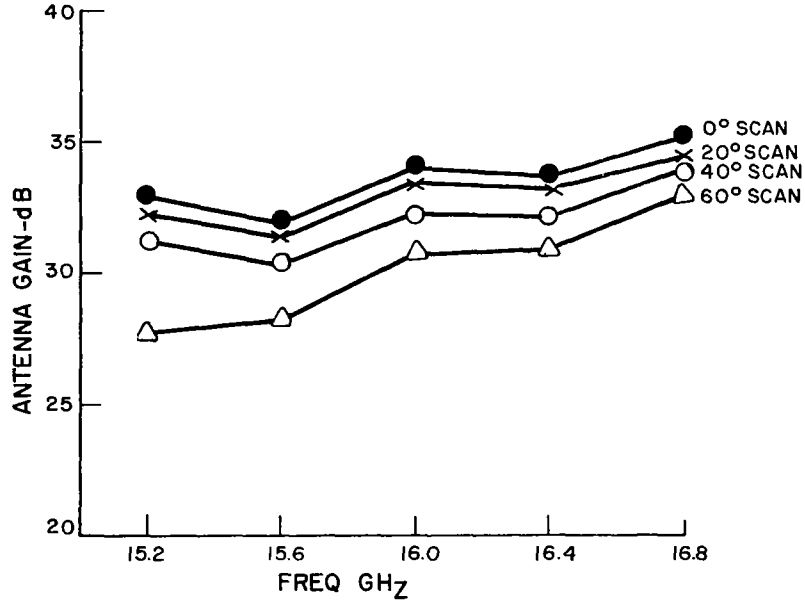

Figure 17. Antenna Gain vs Frequency

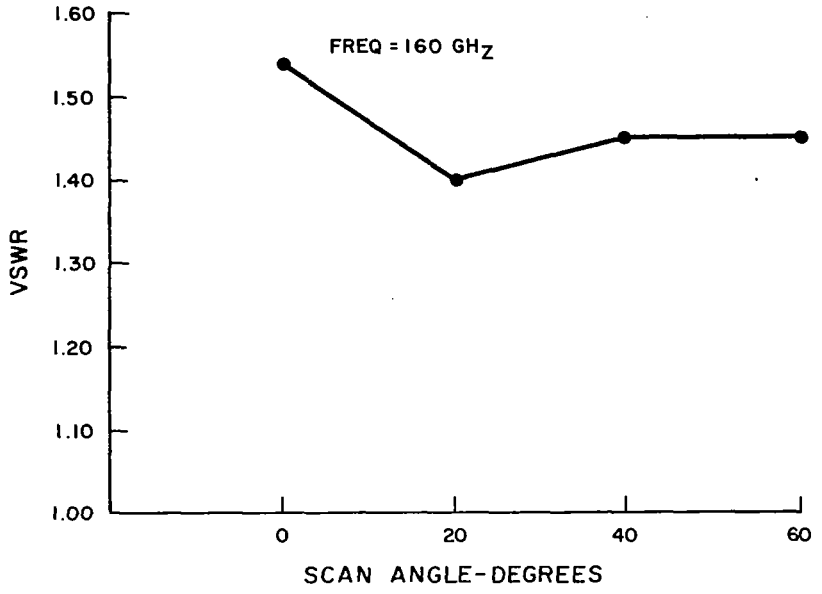

Figure 18. Array VSWR vs Scan Angle (16.0 GHz)

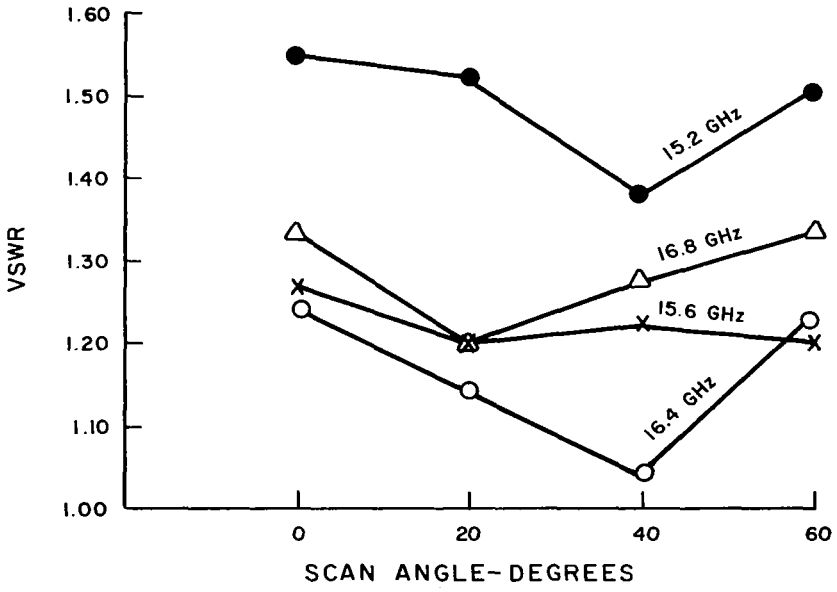

Figure 19. Array VSWR vs Scan Angle

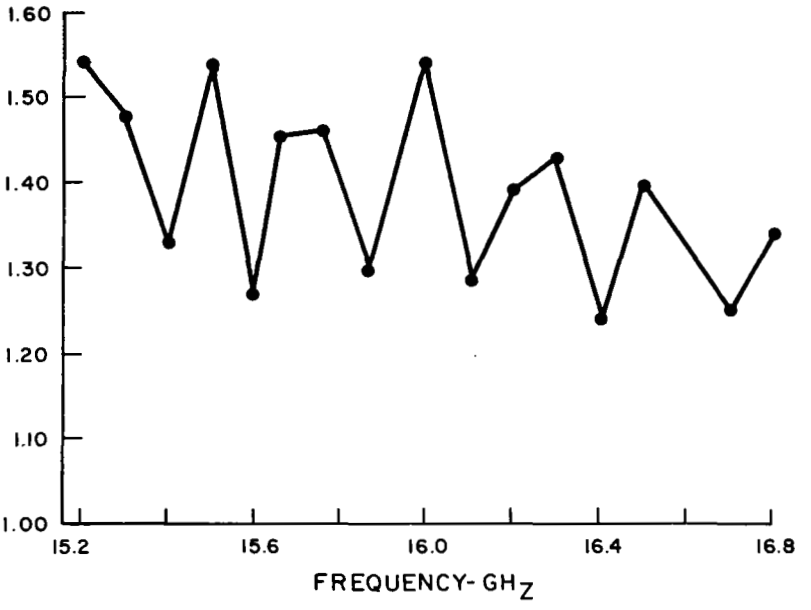

Figure 20. Combiner-Phase Section VSWR vs Frequency

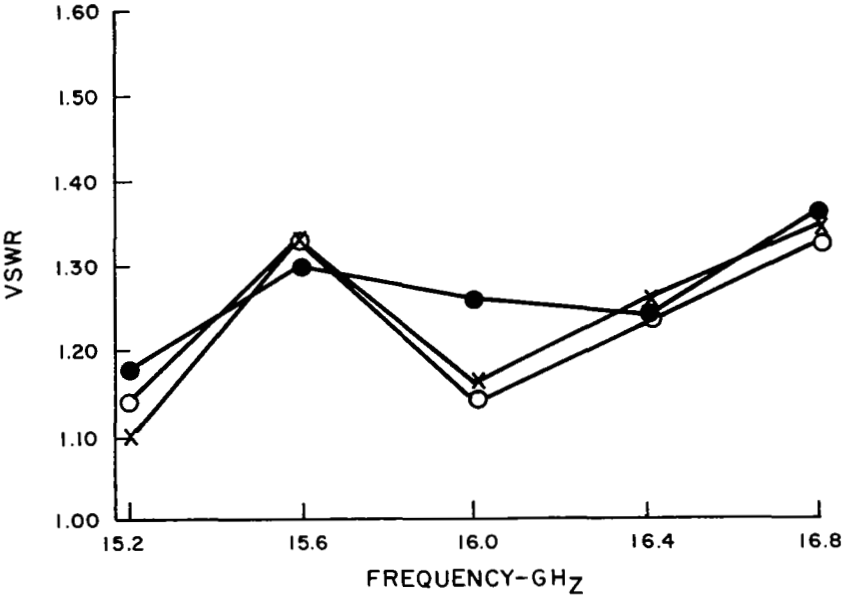

Figure 21. Element VSWR vs Frequency

CONCLUSIONS

Radiation characteristics of the prototype 50-element low-sidelobe phased array were determined for operation over the 15.2 to 16.8 GHz frequency band.

A single-plane scan capability of $\pm 60^{o}$ has been demonstrated with no visible grating lobe or array resonance effects at the selected scan angles and frequencies.

Maximum sidelobe levels in the scan plane ranged from −28 dB at broadside to −18 dB at 60^{o} scan for mid-band operation. Maximum sidelobes in the plane of the line source elements ranged from −40 dB at broadside to −32 dB at 60^{o} scan.

Array beam efficiency at mid-band was a maximum of 98.6% at broadside decreasing to 84.7% as the beam scanned to 60^{o}. Beam efficiency characteristics were only slightly reduced at other frequencies in the 10% band.

The array gain at mid-band was found to be approximately 0.4 dB less than that expected from a lossless array with similar illumination characteristics. Mid-band antenna gain was 33.8 dB.

H-plane patterns and impedance of the line source element were found to be relatively insensitive to its location within the array. The VSWR of the complete antenna did not change appreciably as the beam was scanned.

REFERENCES

1. C. E. Profera: Phased Arrays for Meteorological Satellite. Interim Report prepared for NASA-ERC, June 1967, NASA–CR–86000.

2. C. E. Profera: Phased Arrays for Meteorological Satellite. Interim Report prepared for NASA-ERC, June 1968, NASA–CR–86089.

3. L. H. Yorinks: Feasibility Study for a 60 GHz Radiometric Array. Interim Report prepared for NASA-ERC, January 1969.

4. T. Morita and S. B. Cohn: Microwave Lens Matching by Simulated Quarter-Wave Transformers. Trans. IRE, Vol. AP–3, January 1956.

5. C. J. Miller: Minimizing the Effects of Phase Quantization Errors in an Electronically Scanned Array. Proc. of Symposium on Electronically Scanned Array Techniques and Applications, RADC TDR 64–225, Vol. I, July 1964.

6. H. Jasik Ed.: Antenna Engineering Handbook. Chap. 14, McGraw–Hill, 1961.

7. C. G. Montgomery: Technique of Microwave Measurements. Chap. 10, Radiation Laboratory Series, Vol. 11, McGraw–Hill, 1947.

NASA-Langley, 1969 — 7 CR-1471